Energy Conversion and Management 325 (2025) 119407

Contents lists available at ScienceDirect

Energy Conversion and Management

journal homepage: www.elsevier.com/locate/enconman

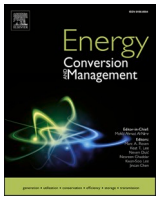

Research Paper

The influence of applying turbine inlet air cooling to a small-scale parallel-flow Brayton cycle

C.C. Cockcroft, W.G. Le Roux *

Department of Mechanical and Aeronautical Engineering, University of Pretoria, Private Bag X20, Hatfield, Pretoria 0028, South Africa

ARTICLE INFO

Keywords:
Brayton cycle
Gas turbine
Microturbine
Parallel-flow
Turbocharger
Turbine inlet air cooling

ABSTRACT

To improve an open air-operated parallel-flow Brayton cycle, the air entering the compressor inlet can be cooled via the concept of turbine inlet air cooling (TIAC). This work investigates whether TIAC forms a worthwhile improvement to the power output and thermal efficiency of a parallel-flow Brayton cycle. An analytical approach is followed to compare the results between a low-temperature turbine (LTT) setup and a similar setup with an added cooling loop for the TIAC concept, considering different crossflow condenser dimensions. A range of commercial turbochargers are used to model the compressor and turbines and the best turbocharger combinations are considered for further analysis. Considering the same pressure ratio, the TIAC cycle does not offer better power output nor thermal efficiency than the LTT cycle, however, it is able to lower the required gasifier turbine inlet temperature (which may not exceed 1200 K due to turbomachinery manufacturer limits). When comparing the LTT and TIAC cycles at their optimum operating points, which shifts to a higher compressor pressure ratio for the TIAC cycle due to a larger TIAC compatibility range, the TIAC layout obtains 64.9 % more power output and a 31.4 % improvement in thermal efficiency for the combination between the G25-550 (AR = 0.92) main shaft turbocharger and the GBC14-200 power turbine. It is recommended to investigate recuperated and solar cycle configurations for further cycle thermal efficiency improvements.

1. Introduction

Air-operated open gas turbine cycles that are used for the generation of electricity are susceptible to changes in the temperature of the ambient air [1]. An increase in the temperature of the ambient air, as the intake air, results in a substantial decline in the power output of a gas turbine cycle [2]. Under warm weather conditions, the power generated via a gas turbine cycle can face reductions of 30 % with a subsequent thermal efficiency decline of 5 %. This indicates a need to improve the performance of gas turbine cycles in warm weather conditions [3]. As a result of a temporal location dependency on the output of a combined heat and power system, factors such as ambient temperature on an hourly basis, thermal grade, and elevation, all effect the output capacity of a power generation system [4]. According to Ref. [5], when comparing the influence of ambient temperature, relative humidity, and pressure on gas turbine functionality, ambient temperature has the greatest influence on the operation of the cycle. A 1 K increase in the ambient temperature can result in a 0.6 % reduction in the power output and a 0.18 % reduction in the thermal efficiency of the cycle [5]. This effect is further intensified when greater cycle pressure ratios are used [5]. Most gas turbines are designed based on an ambient temperature of 15 °C as per standards of the International Organization for Standardisation (ISO) [6]. As an example, for the operation of a gas turbine in Pretoria, South Africa, the region already experiences high ambient temperatures and additional hot weather days, with temperatures above 35 °C, are expected to increase by 49 days by 2050 [7]. These high ambient temperatures need to be accounted for [8].

Many rural communities in southern Africa cannot utilise the electricity supplied by the national energy grid [9]. It is for this reason that researchers are improving and developing a small-scale solar thermal Brayton cycle to meet this energy supply crisis [10]. The regions of application of this small-scale cycle are also susceptible to high ambient temperatures. Thus, there is a need for the application of turbine inlet air cooling (TIAC) to reduce the cycle intake temperature and to subsequently improve the cycle output [3]. TIAC is used to provide cooling to the inlet of a gas turbine cycle via cooling the compressor inlet of the cycle. This is done so that the influence of higher ambient temperatures is negated so that the loss in power output and thermal efficiency at higher ambient temperatures can be reduced [11]. This results in a higher cycle power output due to a lower compressor power input requirement [12]. The concept of TIAC is essentially a modification of

* Corresponding author.
E-mail address: willem.leroux@up.ac.za (W.G. Le Roux).

https://doi.org/10.1016/j.enconman.2024.119407
Received 6 September 2024; Received in revised form 22 November 2024; Accepted 11 December 2024
Available online 21 December 2024

Nomenclature

Symbols

AFR	Air-fuel ratio
D	Diameter [m]
d_t	Turbine exducer diameter [m]
f	Friction factor
H	Height [m]
h	Specific enthalpy [J/kg]
$\dot{I}$	Irreversibility rate (or exergy destruction) [W]
K	Loss coefficient
k	Ratio of specific heats
L	Length [m]
M	Molecular mass [kg/mol]
$\dot{m}$	Mass flow rate [kg/s]
N	Number
N	Rotational speed [RPM]
N_L	Number of tube rows in the same flow direction
n	Number of tubes
$\dot{n}$	Molar flow rate [mol/s]
P	Pressure [Pa]
p	Proportion of pressure drop
$\dot{Q}$	Heat transfer rate [W]
r	Pressure ratio
S	Pitch [m]
s	Specific entropy [J/kgK]
$\dot{S}_{gen}$	Entropy generation rate [W/K]
T	Temperature [K]
t	Thickness [m]
V	Velocity [m/s]
W	Width [m]
$\dot{W}$	Rate of work [W]
x	Proportion of theoretical air

Greek symbols

η	Efficiency
θ	Angle [rad]
ρ	Density [kg/m^3]

Subscripts

0–6	States 0–6
AF	Actual flow
air	Air
CC	Combustion chamber
CF	Corrected flow
comp	Compressor
cond	Condenser
D	Diagonal
e	Electrical
exh	Exhaust
exp	Expander
g	Gas
gen	Generator or generated
gt	Gas turbine
h	Hydraulic
i	Inner
in	Inlet
LPG	Liquified petroleum gas
mass	Mass basis
max	Maximum
mc	Mixing chamber
mole	Molar basis
o	Outer
out	Outlet
pt	Power turbine
red	Reducer
s	Isentropic
shell	Shell
T	Transverse
t	Turbine
th	Thermal
tube	Tube
w	Water

Abbreviations

AR	Aspect Ratio
E	Electrical
GT	Gasifier Turbine
LPG	Liquefied Petroleum Gas
LTT	Low-Temperature Turbine
NTU	Number of Transfer Units
OD	Outer Diameter
PT	Power Turbine
RPM	Revolutions Per Minute
TIAC	Turbine Inlet Air Cooling

improving the performance of a gas turbine cycle through intercooling, as done using various different methods in Refs. [13,14,15]. Both TIAC and intercooling seek to cool the inlet of the compressor of the gas turbine cycle to improve the performance of the cycle, through improving the performance of the compressor. This is further verified in the study by Liu et al. [16], where an improvement in the compressor performance allows for overall better performance in a gas–liquid compressed CO_2 based energy storage system. Additionally, Zhang et al. [17] have determined that system efficiency is greatly dependent on the efficiencies of air turbines and air compressors.

In further justification of the use of TIAC to improve the operation of a gas turbine cycle, Moradi et al. [18] have analysed a TIAC system that utilises hybrid cooling. In this system, the average yearly power output improvement is 6.72 %, with an improvement range of between 3.57 % and 10.6 % in the year depending on the ambient conditions [3]. Similarly, the thermal efficiency improvement is on average 2.4 %, with an improvement range of between 1.15 % and 4.49 % [3]. The lower bound of the improvement range occurs in colder months but shows that TIAC is not only applicable during periods of warm weather but can improve the cycle during colder periods of the year as well [3]. In a similar study by Zaki et al. [19], TIAC has been applied to a gas turbine cycle operating at an ambient temperature of 45 °C where the relative humidity of the ambient air is 43.4 % [19]. In this study, the inlet air to the compressor is lowered to less than the ISO standard with a subsequent improvement of 19.58 % in the cycle power output but with a reduction in the thermal efficiency of up to 5.76 % [19]. This implies that there is a trade-off between thermal efficiency and power output in a TIAC cycle [19].

Furthermore, for regions with poor accessibility to power generation infrastructure and without adequate microturbine manufacturing industries there are high expenses, in the form of taxes and exchange rates, associated with sourcing microturbines for power generation [20]. To combat this issue, commercial automotive turbochargers form a viable substitute for the microturbine in a cycle setup. This concept has been used in the studies by Le Roux & Meyer [21], De Beer et al. [22], Le Roux & Sciacovelli [10], and in the study by Visser et al. [23] which has been adapted into a commercial power generation product.

Small-scale radial turbomachinery, developed from automotive

turbochargers, has advantages over large-scale systems as a result of reduced weight, lower costs, and minimised losses resulting from mechanical friction [24]. The use of a turbocharger that has been modified to operate as the microturbine in a power plant also allows for ease of integration with other components for cogeneration or solar hybridisation [25]. This is greatly due to the radial flow structure of the automotive turbochargers allowing for enough space to integrate the components required to construct the hybridised or cogeneration power plant [26]. In an axial flow arrangement, the combustion chamber is integrated into the compressor and turbine which means that there is not enough space for the addition of components required for cogeneration or solar hybridisation [27]. However, these turbomachines, consisting of automotive turbochargers, operate at relatively low pressure ratios and therefore their performance is sensitive to the addition of pressure drop components to the flow stream [28].

Gas turbine cycles that utilise a two-shaft layout, with turbines in series, are advantageous when operational flexibility is required due to continual load variations through the use of two turbines [29]. In addition to this, the second turbine can operate at an independent shaft speed to only generate the power output of the cycle [29]. However, for a small-scale turbocharger that has been modified to form a microturbine operating at low pressure ratios, this series two-shaft layout is not a viable option for operation. This is due to the reduced pressure ratios through both the turbine that powers the compressor and through the turbine that generates the power. To solve this issue, Van der Merwe et al. [20] have investigated and found feasibility for a two-shaft parallel flow low-temperature turbine (LTT) cycle wherein the pressure ratios through the turbines are not reduced as much as in a standard series two-shaft layout. This lower reduction of the pressure ratios through the turbines allows for further solar hybridisation and cogeneration applications as the additional components do not impact the cycle power output potential significantly. This LTT cycle can utilise two automotive turbochargers since the gasifier turbine is coupled to the cycle compressor (this combination is known as a turbocharger per definition) and the low-temperature power turbine is attached, in parallel, to a generator (which is a turbocharger without a compressor wheel and coupled to a generator) [20].

1.1. Novelty and originality of this work

Commercial automotive radial turbochargers form a viable solution to developing an LTT micro-turbine setup while maintaining the advantages of a series twin-shaft cycle. Such a setup also has an advantage when it comes to hybridisation with renewable energy sources, such as concentrating solar power and cogeneration. However, in regions with warm climates the efficiency and power output of the cycle can be improved through cooling the inlet air to the cycle via the use of turbine inlet air cooling (TIAC). In the current work, a modification of a TIAC concept, as presented by Zaki et al. [19], is to be directly compared to an updated model of the LTT setup by Van der Merwe et al. [20]. This is done to determine whether TIAC forms a worthwhile cycle addition to improve the thermal efficiency of the LTT parallel-flow cycle. The novelty of the current study is formed through comparing these two cycles and through the incorporation of commercial *Garrett Motion* [30] turbochargers into the coupled cycle layouts. Additionally, a consideration of the exergy destruction that occurs in the cycle operation of each component in the LTT and TIAC cycles is also addressed. Additional novelty is formed as a result of the generator in the current study being coupled to the parallel expander. This is in contrast to the study by Zaki et al. [19] in which the generator was coupled to the gasifier turbine with the parallel expander having the purpose of reducing the pressure in the cooling cycle loop while supplying some of the power with an additional generator. Lastly, the current study also adds novelty through the addition of water heating for cogeneration, through a consideration of different crossflow condenser dimensions, while cooling the air flowing to the power turbine in the TIAC setup. This water heating is not included in the LTT cycle. The consideration of different condenser geometries is further different to the study by Zaki et al. [19] where component geometries have not been considered.

2. Methodology

The methodology in this study consists of an introduction into the LTT and TIAC cycle layouts and an analysis of the equations and setups pertaining to each component in the cycles. Hereafter, the solution algorithms of the cycles are introduced and explained so that the setups can be analysed and discussed.

2.1. Cycle layouts

This study seeks to investigate and compare two gas turbine layouts. The first layout is for the low-temperature turbine (LTT) setup illustrated in Fig. 1. This layout involves an air intake at state 1 which undergoes a compression process that exits at state 2. After state 2, the flow splits to the power turbine and to the remainder of the cycle components. Hereafter, the cycle undergoes a heating process from state 2 to state 3 through the injection and combustion of fuel into the cycle air. The final process after the combustion chamber is the expansion of the newly formed gas mixture in the gasifier turbine, from state 3 to state 4, whereafter the gas mixture exhausts to the atmosphere. In the remaining split path, from state 2 to state 5, the power turbine undergoes an expansion process to generate power in the cycle. The air is then exhausted to the atmosphere after state 5. The cycle requires a certain amount power to operate the compressor (compression from state 1 to state 2), coming directly from the coupled gasifier turbine (expansion from state 3 to state 4). These power amounts equate to one another. The net power output of the cycle comes from the power generation process in the power turbine which is further utilised through the generator that is coupled to the power turbine.

The second layout is for the turbine inlet air cooling (TIAC) layout as visualised using Fig. 2. In this layout, states 1 to 4 follow the same setup as in the LTT layout, but the split-off point after state 2 is succeeded by a condenser prior to the power turbine inlet. The power turbine is followed by a mixing chamber that mixes the process air with the ambient air that enters the cycle at state 0 before entering the compressor at state 1. The process for these extra components follows a loop, whereupon the condenser cools the air from state 2 to state 5. Hereafter the power turbine generates the power output through an expansion process from state 5 to state 6 and subsequently cools the air further so that the cooled

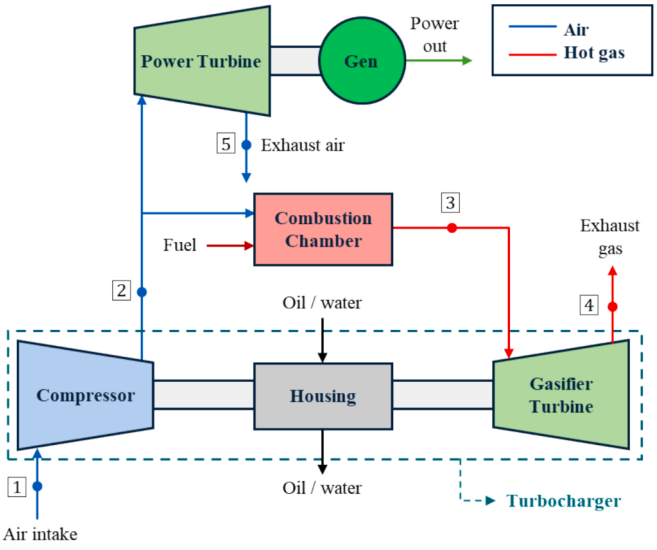

Fig. 1. Low-temperature turbine (LTT) layout.

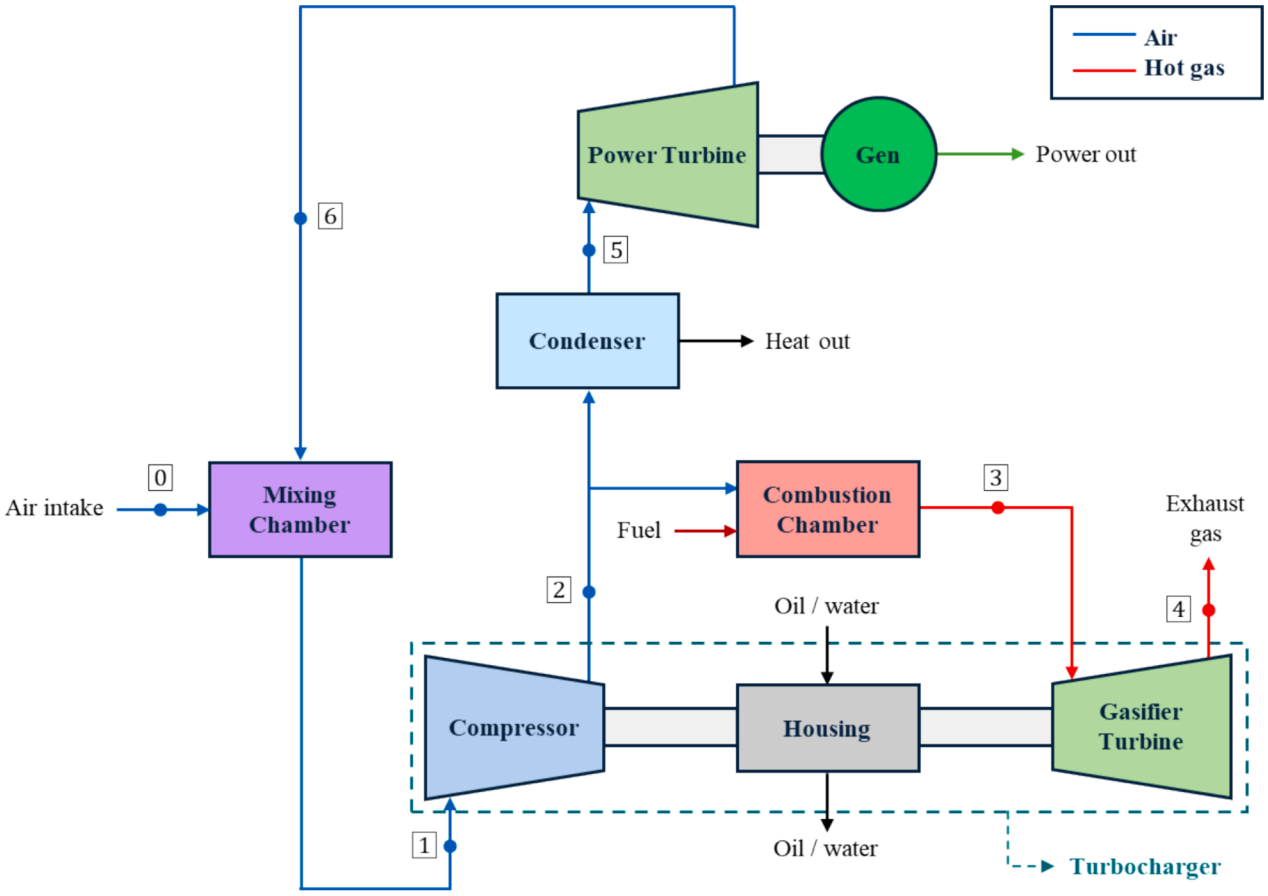

Fig. 2. Turbine inlet air cooling (TIAC) layout.

air entering the mixing chamber at state 6 can lower the temperature of the compressor inlet using the mixing chamber.

For both the LTT and TIAC cycle layouts, the net power output and the thermal efficiency are determined using the same relations. The thermal efficiency equates to the ratio between the net power output (from the power turbine) and the heat associated with the use of the combustion chamber. The relation used to determine the power output is determined as per Equation (1) and the thermal efficiency is determined as per Equation (2).

$$\dot{W}_{net} = \dot{W}_{gt} + \dot{W}_{pt} - \dot{W}_{comp} = \dot{W}_{pt} \tag{1}$$

$$\eta_{th} = \frac{\dot{W}_{net}}{\dot{Q}_{CC}} \tag{2}$$

2.2. Component analysis

Following from the layouts of the LTT and TIAC setups, five processes and their associated components are modelled in terms of their associated equations for a steady-state analysis of the cycles. This is done in the sub-sections to follow. CoolProp, an open-source property library, is used to characterise the properties of states associated with the equations in this study [31]. The cycle layouts are then solved via Python coding algorithms. Each component is also considered in terms of the exergy destruction (irreversibility) that occurs through the operation of the component or process. This exergy destruction is inevitable in a real-world thermodynamic cycle and is responsible for the loss of available work in the cycle.

2.2.1. Compressor and turbines

There are three components that are characterised in each cycle using commercial turbochargers. These components are the adiabatic coupled compressor and gasifier turbine as well as the parallel shaft adiabatic power turbine. For this, different commercially available *Garrett Motion* turbochargers are considered for the different layouts [30]. Seeing as commercial turbochargers are used, the equations and values pertaining to these turbocharger components are directly obtained from flow maps provided by the turbocharger manufacturer. This means that the only changes associated with the use of these turbochargers arise from the use of different turbochargers and different pressure ratios for simulation [32]. Additionally, *Garrett Motion* turbochargers are subject to an allowable turbine inlet temperature of no greater than 950 °C [33]. This is accounted for in the current study through a conservative maximum temperature limit of 1200 K (927 °C).

When grouping the compressor and gasifier turbine together to form a turbocharger, these components are connected via the same shaft and can also be coupled to a generator to achieve steady state, as discussed in depth by Ref. [20]. For the gasifier, the procedure for obtaining values that pertain to a paired compressor and turbine, as per the *Garrett Motion* turbocharger catalogue [30], starts with obtaining the corrected mass flow rate for the turbine. This is done under the consideration of a specific turbine pressure ratio, from the catalogue exhaust flow map, as illustrated in Fig. 3. It is also important to note the maximum turbine efficiency as provided by the manufacturer. From this, the actual mass flow rate can be determined using Equation (3) [32]. The corrected compressor mass flow rate is then determined via Equation (4) [32].

$$\dot{m}_{comp,AF} = \dot{m}_{gt,CF} \frac{\left(\frac{P_{gt,in}}{14.7\times 6894.8}\right)}{\sqrt{\frac{\left(\left(T_{gt,in}-273.15\right)\times 1.8+492\right)}{519}}} \tag{3}$$

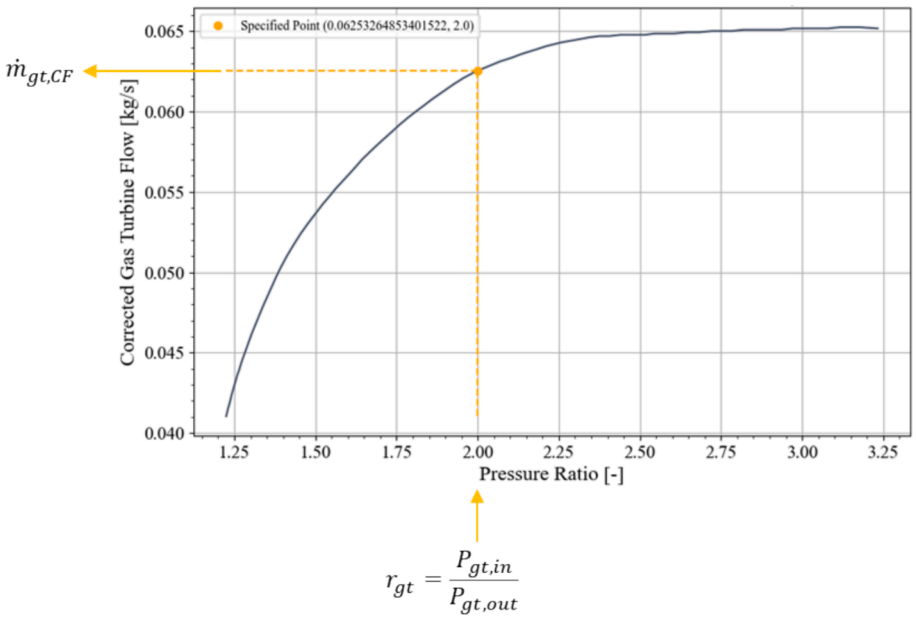

Fig. 3. Exhaust flow chart for determining the corrected turbine mass flow rate at a selected pressure ratio.

$$\dot{m}_{comp,CF} = \dot{m}_{comp,AF} \frac{\sqrt{\frac{\left(\left(T_{comp,in} - 273.15\right) \times 1.8 + 492\right)}{545}}}{\left(\frac{P_{comp,in}}{13.95 \times 6894.8}\right)} \tag{4}$$

Following from Equation (3) and (4), via the use of the corrected compressor mass flow rate and the compressor pressure ratio, the compressor map can be used to obtain values for the shaft speed and for the compressor efficiency. A Python contour map is used to do this in two parts as shown in Fig. 4 and Fig. 5. This completes the characterisation of the compressor via the manufacturer flow maps. It is important to make sure that the operational mass flow rate and compressor pressure ratio falls within the bounds of the compressor map as flow surges or choking occurs beyond this region [32].

With the known values, under the consideration of the turbine exducer diameter as provided by the turbocharger manufacturer, the blade speed ratio is calculated as per Equation (5). CoolProp is used to determine the required gasifier turbine inlet specific enthalpy for the determination of the blade speed ratio. For this, updated air reference

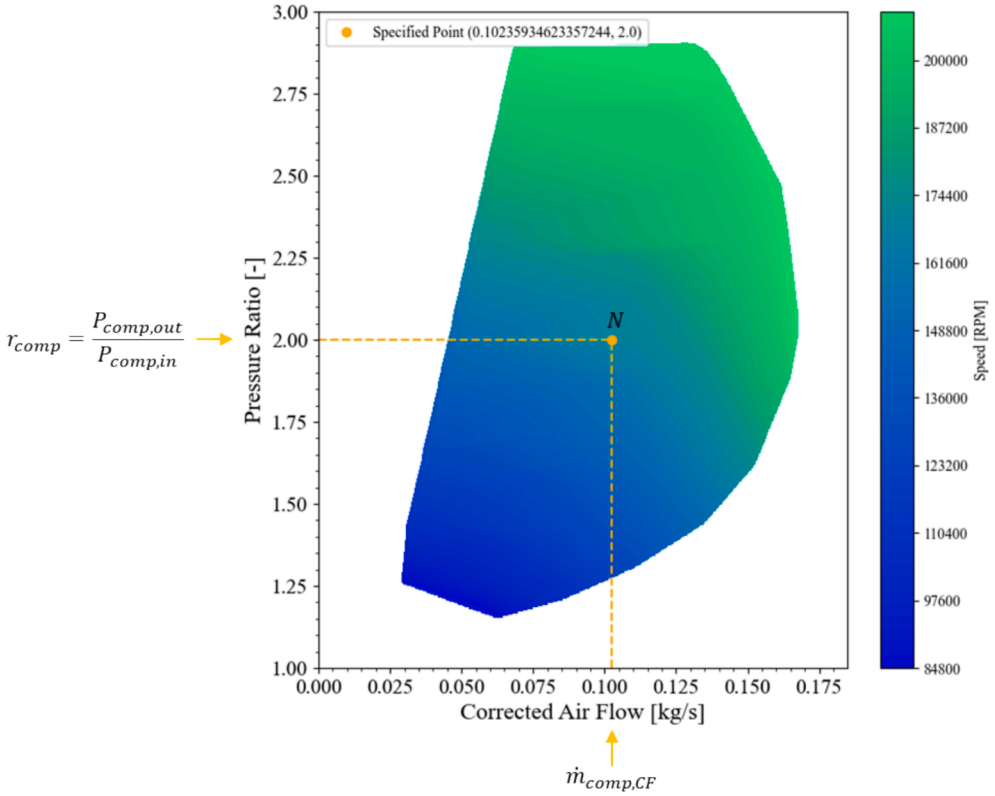

Fig. 4. Compressor map for determining the rotational speed at a selected pressure ratio.

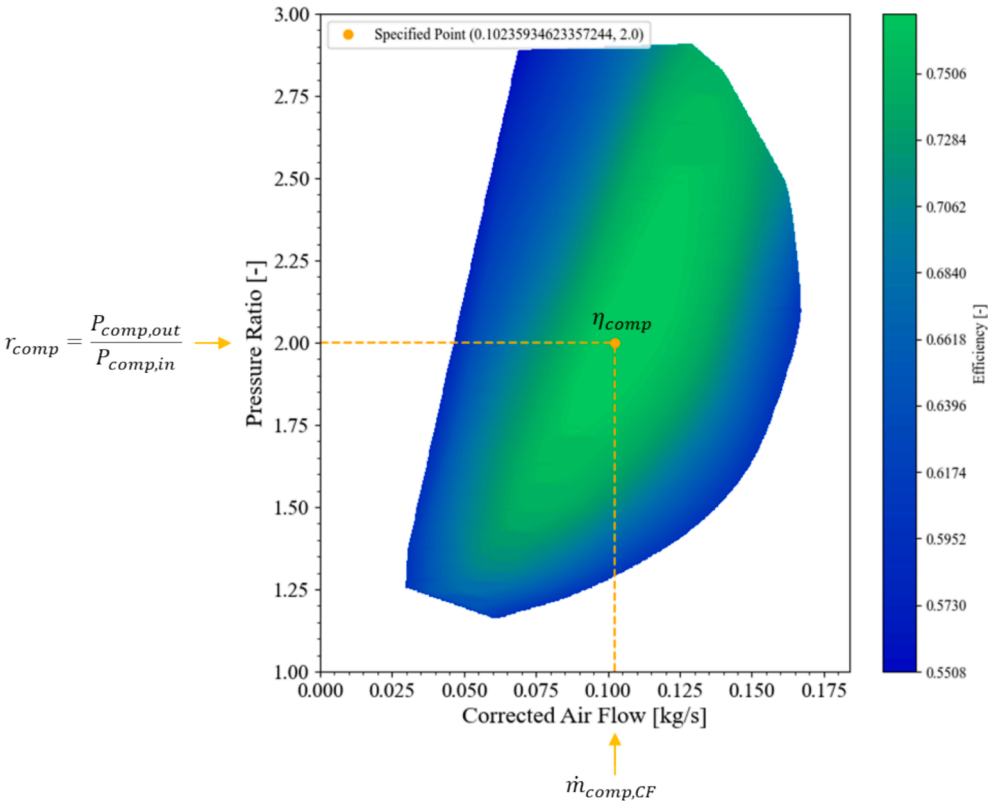

Fig. 5. Compressor map for determining the compressor efficiency at a selected pressure ratio.

states as per Borgnakke & Sonntag [34] are used in an iterative solution procedure. Using the newly calculated blade speed ratio and the noted maximum turbine efficiency, Equation (6) is used to determine the actual efficiency of the turbine [32].

$$BSR = \frac{\left(\frac{2\pi N}{60}\right) \times \left(\frac{d_{gt}}{2}\right)}{\sqrt{2 \times h_{gt,in}\left(1 - \left(r_{gt}\right)^{\frac{1-k_g}{k_g}}\right)}} \tag{5}$$

$$\eta_{gt} = \eta_{gt,max} \times \left[1 - \left(\frac{BSR - 0.6}{0.6}\right)^2\right] \tag{6}$$

The cycles modelled and simulated in this study entail changing inputs and iteration procedures. Additionally, initial values are assumed for the gasifier turbine inlet temperature, for the mass flow rates associated with the combustion process that occurs before the gas enters the gasifier turbine, and for the pressure at the turbine inlet when pressure loss components precede the turbine. Thus, the compressor and exhaust flow maps are converted, via *WebPlotDigitizer* [35], into a useful digital format that can be interpolated from for the iteration procedures [20].

Following from the values obtained and iterated for from the turbocharger maps, the outlet enthalpy associated with the compressor can be determined using Equation (7) and via determining the isentropic outlet enthalpy using the entropy at the inlet of the compressor. The outlet temperature is determined from the actual outlet enthalpy using CoolProp. Similarly, the outlet enthalpies of the gasifier turbine can be determined as per Equation (8) [34].

$$h_{comp,out} = \frac{h_{comp,out,s} - h_{comp,in}}{\eta_{comp}} + h_{comp,in} \tag{7}$$

$$h_{gt,out} = h_{gt,in} - \eta_{gt}\left(h_{gt,in} - h_{gt,out,s}\right) \tag{8}$$

The next procedure is to determine the work rates associated with the compressor and gasifier turbine. This is done using Equations (9) and (10), respectively, as per an energy balance analysis [20]. However, even though the equations for the cycle mass flow rates have been introduced, the actual gasifier turbine mass flow rate depends on the mass flow rate associated with the fuel that is injected into the cycle as this fuel influences the results of a gas cycle [36]. Provision is made for this and discussed in the combustion chamber analysis.

$$\dot{W}_{comp} = \dot{m}_{comp,AF}\left(h_{comp,out} - h_{comp,in}\right) \tag{9}$$

$$\dot{W}_{gt} = \dot{m}_{gt}\left(h_{gt,in} - h_{gt,out}\right) \tag{10}$$

In terms of the equations associated with the power turbine, the analysis is the same as for the connected compressor and gasifier turbine. However, the actual turbine mass flow rate replaces the virtual compressor mass flow rate. This is because there is no cycle split or LPG injection in the coupled power turbine and generator analysis. Note that the generator power and speed are determined by simulating a virtual compressor coupled to the turbine as per Ref. [18].

Lastly, the entropy generation rates in the non-isentropic turbomachinery components, as functions of specific entropy, are used to determine the irreversibility rates in these components. This is done for the purpose of an exergy analysis for both the LTT and TIAC cycles. The exergy destruction rate is thus determined via Equation (11) for the compressor, via Equation (12) for the gasifier turbine, and via Equation (13) for the power turbine.

$$\dot{I}_{comp} = T_0\dot{S}_{gen,comp} = T_0\dot{m}_{comp}\left(s_{comp,out} - s_{comp,in}\right) \tag{11}$$

$$\dot{I}_{gt} = T_0\dot{S}_{gen,gt} = T_0\dot{m}_{gt}\left(s_{gt,out} - s_{gt,in}\right) \tag{12}$$

$$\dot{I}_{pt} = T_0\dot{S}_{gen,pt} = T_0\dot{m}_{pt}\left(s_{pt,out} - s_{pt,in}\right) \tag{13}$$

2.2.2. Combustion chamber

For the combustion process, an air–fuel mixture is formed in the

combustion chamber through the injection of fuel. Liquefied petroleum gas (LPG) is considered as the fuel in the current study. As per LPG formulation in South Africa, this fuel consists of 60 % propane and 40 % butane [37]. This results in a fuel molecule that is approximated as $C_{3.4}H_{8.8}$.

For a realistic combustion process, excess air is expected to be found in the combustion mixture [38]. Thus, the chemical reaction equation for the combustion chamber, considering an unknown amount of air, is as per Equation (14), with x being used to represent the decimal of the theoretical air. For reference, when the theoretical air decimal equates to one, there is 100 % theoretical air in the mixture.

$$C_{3.4}H_{8.8}+5.6x(O_2+3.76N_2)\rightarrow 3.4CO_2+4.4H_2O+5.6(x-1)O_2+21.056xN_2 \quad (14)$$

Following from the known chemical reaction equation, the mass flow rate associated with the combustion fuel can be determined. This mass flow rate is used to determine the relation between the air mass flow rate before combustion and the mass flow rate of the gas mixture after combustion as per a mass flow rate balance. For this the air–fuel ratio on a mass basis is determined via Equation (15) so that the fuel mass flow rate can be determined as per Equation (16). The mass balance relation, under a consideration of the control volume of the combustion chamber as per Fig. 6, is presented in Equation (17) for the mass flow rates associated with the combustion chamber. In Equation (17) the term on the left-hand side represents the mass flow rates leaving the combustion chamber and the right-hand terms represent the mass flow rates entering the combustion chamber [34].

$$AFR_{mass} = AFR_{mole}\frac{M_{air}}{M_{LPG}} = \frac{\dot{n}_{air}}{\dot{n}_{LPG}}\frac{M_{air}}{M_{LPG}} \quad (15)$$

$$\dot{m}_{LPG} = \frac{\dot{m}_{comp} - \dot{m}_{pt}}{AFR_{mass}} \quad (16)$$

$$\dot{m}_{gt} = \left(\dot{m}_{comp} - \dot{m}_{pt}\right) + \dot{m}_{LPG} \quad (17)$$

To determine the outlet temperature of the combustion chamber, the process of solving for the adiabatic flame temperature, as per Borgnakke & Sonntag [34], is followed. An iterative procedure is used for this to obtain the outlet temperature of the combustion chamber that would allow for the gasifier turbine's generated power to equal the power required to operate the compressor. The adiabatic flame temperature required for this operation is dependent on the pressures and temperatures of the entering fuel, the entering air, and exiting gas mixture associated with the combustion chamber. Through this iterative process, the required theoretical air percentage is solved for. Note that no consideration has been made for heat loss to the environment in the combustion chamber. Thus, it is assumed that the combustion chamber is well-insulated. Additionally, enthalpy values are required for calculation in this solution procedure, with these enthalpy values being dependent on the inlet and outlet temperatures and pressures associated with the combustion chamber. Thus, a suitable relation for the combustion chamber pressure drop needs to be used to determine the outlet pressure of the combustion chamber [34].

For the determination of the combustion chamber pressure drop, the pressure drop is considered to be a proportion of the pressure of the air entering the combustion chamber. According to Lefebvre & Ballal [38], the pressure drop in an annular-tube or annular combustion chamber is 6 %. Thus, this is the maximum value considered for the pressure drop percentage in the combustion chamber, where the outlet pressure of the combustion chamber is defined as per Equation (18). Note that the proportion of pressure drop in the combustion chamber is taken to be $p_{cc} = 0.06$ for the maximum considered pressure drop.

$$P_{CC,out} = (1 - p_{CC})P_{CC,in} \quad (18)$$

The last variables that need to be calculated for the combustion chamber is the heat transfer rate associated with the combustion process and the irreversibility of the combustion process for exergy analysis purposes. The heat transfer rate is determined via Equation (19) from an energy balance consideration of the combustion chamber as per the control volume diagram in Fig. 6 [34]. The irreversibility rate in the combustion chamber is determined as per Equation (20).

$$\dot{Q}_{CC} = \dot{m}_{gt}h_{CC,out} - \left(\dot{m}_{gt} - \dot{m}_{LPG}\right)h_{CC,in} - \dot{m}_{LPG}h_{LPG,in} \quad (19)$$

$$\dot{I}_{CC} = T_0\dot{S}_{gen,CC} = T_0\left[\dot{m}_{gt}s_{CC,out} - \left(\dot{m}_{gt} - \dot{m}_{LPG}\right)s_{CC,in} - \dot{m}_{LPG}s_{LPG,in}\right] \quad (20)$$

2.2.3. Condenser

The condenser forms an important component in the turbine inlet air cooling (TIAC) cycle. The geometry of this condenser is defined based on a steady-flow crossflow heat exchanger design as illustrated in Fig. 7. A round-to-rectangle expander and a rectangle-to-round reducer are used to link the condenser to its preceding and succeeding components in the cycle as per the linking turbomachinery inlet and outlet diameters. A crossflow design is used for practicality and simplicity in component positioning [39].

The condenser is designed to allow municipal water to flow through the condenser tubes to cool the air flowing through the condenser, with this municipal water having the potential to be used as heated water for domestic use. An inlet water temperature of 20 °C is assumed based on the highest average monthly cold tap water temperatures in Pretoria, South Africa, due to the high ambient temperature used in this study (see section 2.2.5). The warmest average cold water temperature is recorded to be 19.7 °C in February in Pretoria, South Africa [40]. The outlet water temperature is initially unknown and calculated for in the solution procedure (an outlet water temperature of between 38 °C and 42 °C is usually desired for domestic use [41]). In terms of the mass flow rate of the cooling water, according to SANS (South African National Standards) 3088 it is expected that municipal water flows at 5 L/min considering a 600 kPa reference pressure [42]. This results in a mass flow rate of 0.08 kg/s. However, the choice of water mass flow rate is not expected to affect the performance of the TIAC cycle, because the low heat transfer coefficient on the air-side will dominate the overall heat transfer coefficient calculation. It is further assumed that the conditions of the inlet water to the condenser remain constant throughout the operation of the cycle.

For the condenser tubes, copper tubes with a wall thickness of 1 mm are used so that there is minimal thermal resistance created by the tube

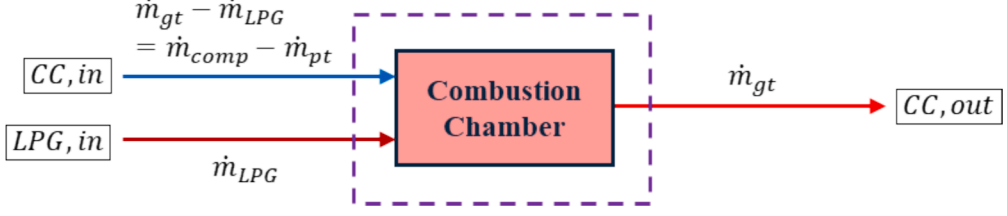

Fig. 6. Control volume of the combustion chamber.

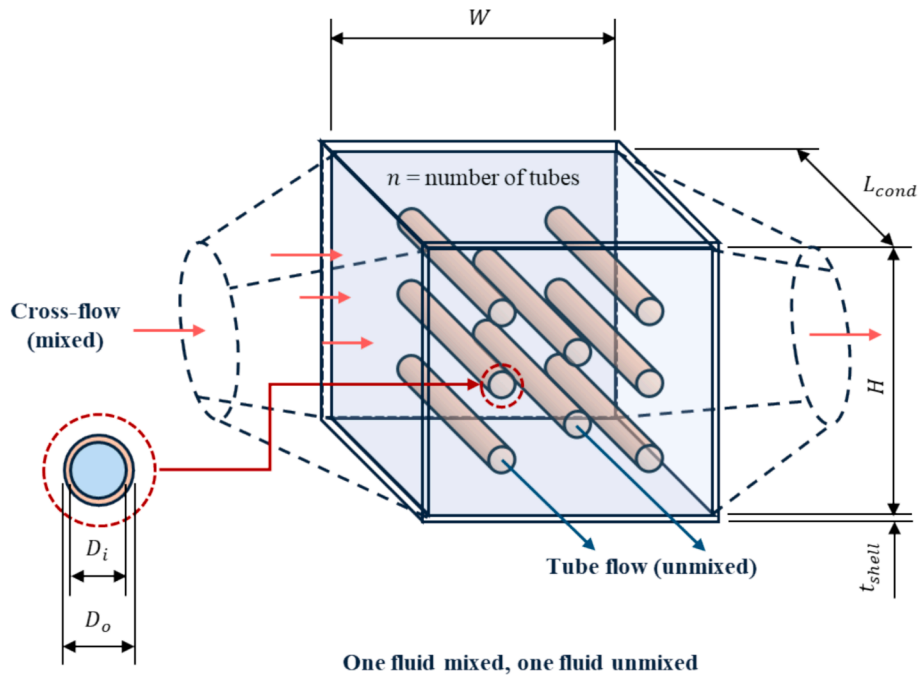

Fig. 7. Condenser geometry and dimensional variables.

walls. Copper tubes are used for their strength, corrosion resistance, and ability to be used under high pressures [43]. In addition to this, the length of the condenser and subsequently the length of the condenser tubes, L_{cond}, is assumed to be 1 m to reduce the number of geometry variables associated with the condenser.

Considering the crossflow geometry of the condenser, as well as the defined geometries and conditions associated with the condenser, the effectiveness-NTU method for solving for a crossflow heat exchanger, as provided by Çengel & Ghajar [44], is used to obtain the unknown values pertaining to the condenser. For this, the condenser tubes are considered in terms of a thermal resistance network with the inclusion of fouling on both the water-side and the air-side of the tubes. The outlet temperatures of the air and water flow streams of the condenser are iterated for in this procedure. Additional considerations are made in addition to the effectiveness-NTU method and are discussed further. One of these considerations is heat loss to the environment, with a second consideration being the pressure drop in the condenser.

To determine the heat loss in the condenser, dimensions need to be determined for the shell of the condenser. It is assumed that the shell is made of stainless steel with a shell thickness of 1 mm. The properties of this stainless steel are based on the properties provided by Çengel & Ghajar [44]. The condenser tubes are assumed to follow a staggered equilateral tube layout with a triangular pitch that equates to 1.25 times the outer diameter of the tubes. The shell clearance is defined as per Thome [45]. The shell width and height are determined based on the tube dimensions and positioning as well as the number of tubes in the layout [45]. Furthermore, to minimise the shell heat loss, the shell is insulated. The insulation properties and thickness is the same as that of the recuperator design by Le Roux & Sciacovelli [10].

For further quantification of the condenser heat loss, correlations for combined and forced convection over a flat plate are used for the ambient air flowing over the condenser shell. In this analysis it is assumed that the average wind speed is 2.5 m/s. The mentioned correlations are utilised based on theory from Çengel & Ghajar [44].

For the condenser shell-side pressure drop, Equation (21) [44] is used, with the loss coefficients defined in Equations (22) and (23) being based on the theory by White [46] with a reduction and expansion angle of 22.5°. The condenser velocity and maximum velocity are determined based on the detailed tube arrangement and can be calculated using Equation (24) and (25) [44]. The friction factors are determined based on the Colebrook equation for friction factors [44]. The hydraulic diameter associated with the shell is determined as per Equation (26) [44].

$$\Delta P = \frac{\rho V_{cond}^2}{2}\left(f_{shell}\frac{W}{D_{h,shell}} + K_{exp} + K_{red}\right) + f_{tube}N_L\frac{\rho V_{cond,max}^2}{2} \tag{21}$$

$$K_{exp} = 2.61 sin\theta_{red} \times \left(1 - \frac{D_{cond,i,in}^2}{D_{h,shell}^2}\right)^2 + f_{avg}\frac{2L_{exp}}{D_{h,shell} + D_{cond,i,in}} \tag{22}$$

$$K_{red} = 0.01 \tag{23}$$

$$V_{cond} = \frac{\dot{m}_{pt}}{\rho N_T S_T L_{cond}} \tag{24}$$

$$V_{cond,max} = \frac{S_T}{2(S_D - D_o)}V_{cond} \tag{25}$$

$$D_{h,shell} = \frac{2HL_{cond}}{H + L_{cond}} \tag{26}$$

Lastly, for the purpose of an exergy analysis, the irreversibility rate in the condenser needs to be determined. This is done based on the specific entropy values associated with the various condenser states as per Equation (27).

$$\dot{I}_{cond} = T_0\dot{S}_{gen,\,cond} = T_0\left[\dot{m}_{cond,air}\left(s_{cond,air,out} - s_{cond,air,in}\right) + \dot{m}_w\left(s_{w,out} - s_{w,in}\right) + \frac{\dot{Q}_{loss}}{T_0}\right] \tag{27}$$

2.2.4. Mixing chamber

A mixing chamber is used to cool the ambient air so that the temperature of the compressor inlet is reduced. The mixing chamber is modelled simply as a cylinder with inlets and outlets associated with the dimensions of the connecting components. Thus, the *Garrett Motion* turbomachinery components greatly dictate the dimensions of the

mixing chamber. Therefore, the diameter used for the mixing chamber inlet, at state 6, is the same as the diameter of the power turbine outlet, and the diameter used for the mixing chamber outlet, at state 1, is the same as the diameter of the compressor inlet. The mixing chamber geometry is defined as in Fig. 8. It is assumed that the length of the mixing chamber is 0.5 m to simplify the analysis. It is also assumed that the flow through the mixing chamber is steady and that there is no exchange of work between the mixing chamber and the surroundings.

The flow through the mixing chamber, the sudden expansions associated with the inlets, as well as the sudden contraction associated with the outlet will contribute to the total pressure drop. For a pressure loss determination, the loss coefficients are based on White [46]. The Colebrook equation is used to determine the friction factor inside the mixing chamber, with the properties of stainless steel being used for the determination of the relative roughness of the pipe. Note that the two entering mass flow rates are considered separately for the pressure drop, and thus the total pressure drop is considered based on two different flow streams in a simple analysis [44]. The total pressure drop is then determined using Equation (28) [44], under the assumption that the two streams entering the mixing chamber are both at ambient pressure, and the subsequent inlet compressor pressure is calculated as per Equation (29).

$$\Delta P = \frac{8\left(\dot{m}_{comp}-\dot{m}_{pt}\right)^2}{\pi^2\rho D_i^4}\left(f\frac{L_{mc}}{D_i}+\left(1-\frac{D_0^2}{D_i^2}\right)^2+0.42\left(1-\frac{D_1^2}{D_i^2}\right)\right)+\frac{8\dot{m}_{pt}^2}{\pi^2\rho D_i^4}\left(f\frac{L_{mc}}{D_i}+\left(1-\frac{D_6^2}{D_i^2}\right)^2+0.42\left(1-\frac{D_1^2}{D_i^2}\right)\right) \quad (28)$$

$$P_1 = P_6 - \Delta P \quad (29)$$

Energy balance principles, along with the use of CoolProp, are used to solve the mass flow rates, enthalpies, and heat transfer rate associated with the mixing flow streams. The outlet enthalpy of the mixing chamber is determined as per Equation (30), with CoolProp being used to determine the temperature value associated with this outlet enthalpy at the outlet pressure (determined using Equation (29)). For this analysis, the thermal resistance network associated with the walls and the insulation surrounding the mixing chamber is considered to quantify the heat gain to the mixing chamber. This is necessary based on the concept that the mixing chamber gains additional heat from the environment. For this, correlations are used pertaining to forced and natured convection over a cylinder and a combination between these convection relations is considered as per Çengel & Ghajar [44], with the same insulation and average wind speed as considered for the condenser. The irreversibility rate of the mixing chamber process is characterised via Equation (31).

$$h_1 = h_0 - \frac{\dot{m}_{pt}(h_1-h_6)+\dot{Q}_{gain}}{\left(\dot{m}_{comp}-\dot{m}_{pt}\right)} \quad (30)$$

$$\dot{I}_{cond} = T_0\dot{S}_{gen,mc} = T_0\left[\dot{m}_0(s_1-s_0)+\dot{m}_{pt}(s_1-s_6)-\frac{\dot{Q}_{gain}}{T_0}\right] \quad (31)$$

2.2.5. Exhaust

It is a requirement that the cycle must exhaust to ambient conditions at each cycle exhaust process. For this, the cycles exhaust to ambient conditions consisting of an assumed atmospheric pressure of 86.6 kPa (for Pretoria, South Africa) and an ambient temperature of 300 K [32]. The irreversibility rate of the exhaust process is determined, for the purpose of an exergy analysis, as per Equation (32).

$$\dot{I}_{exh} = \dot{m}_{exh}[h_{exh}-h_0-T_0(s_{exh}-s_0)] \quad (32)$$

2.3. Low-temperature turbine (LTT) analysis

When it comes to simulating and solving the low-temperature turbine (LTT) cycle, arrays are inputted into Python using different values for the compressor pressure ratio and for the pressure drop percentage in the combustion chamber. A range of compressor pressure ratios from 1.4 to 2.5 and a range of combustion chamber pressure drop percentages from 0 % to 6 % are simulated. Furthermore, the Python code makes use of defined functions to model each of the cycle components. The general format of the solution algorithm is as per Fig. 9. It is noted that there are additional breaks in the algorithm to prevent the code from continually solving loops that do not obtain solutions. This is not indicated in Fig. 9.

2.4. Turbine inlet air cooling (TIAC) analysis

For the turbine inlet air cooling (TIAC) cycle, a Python algorithm is implemented to obtain solutions for the cycle layout. This involves providing input arrays for the compressor pressure ratio, for the number of condenser tubes, and for the outer diameter of the condenser tubes. For this, simulations are done for a range of compressor pressure ratios from of 1.5 to 2.5, for condenser tube outer diameters of 4 mm to 15 mm, and for a range between 15 and 45 condenser tubes. The combustion chamber pressure drop is assumed to be 6 % as per Lefebvre & Ballal [38] for annular combustion chambers instead of using different combustion chamber pressure drop percentages as in the low-temperature turbine (LTT) analysis. Additionally, the general solution procedure for solving the cycle case is illustrated in Fig. 10. This is an iterative process that entails the use of solution breaks to prevent infinite loops.

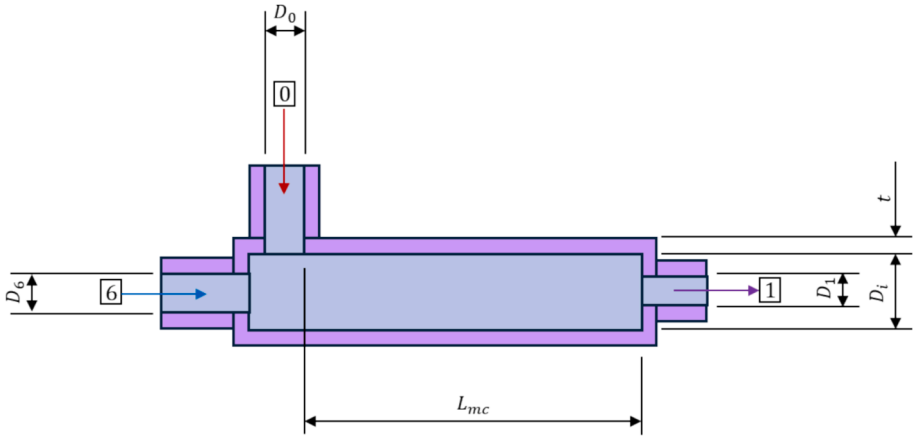

Fig. 8. Mixing chamber geometry and dimensional variables.

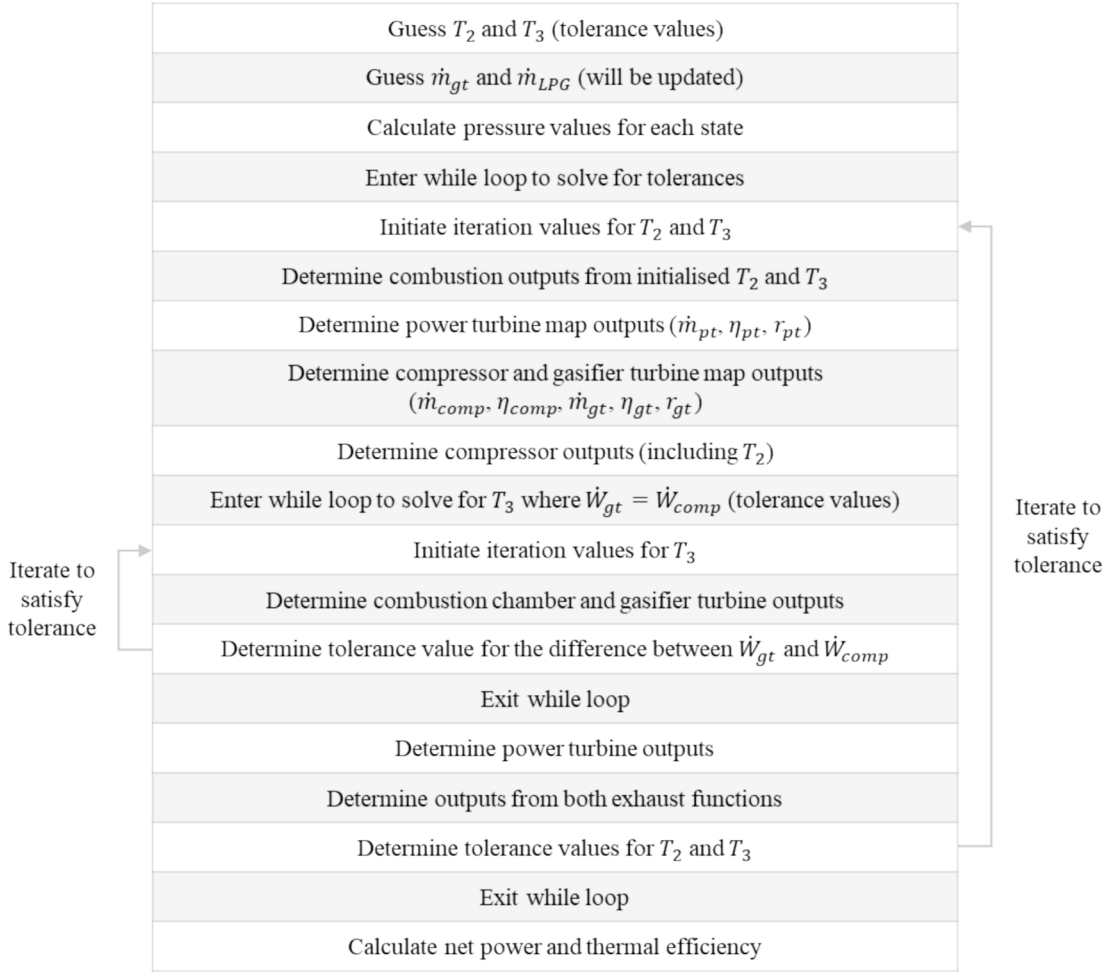

Fig. 9. Low-temperature turbine (LTT) cycle solution procedure.

These breaks are not illustrated in Fig. 10.

3. Results

Following from the methodology pertaining to the two cycle layouts, the cycles are simulated, and the results are summarised in this section. Nine different turbocharger combinations are considered for this and the combination(s) with the best compatibility results is/are discussed prior to a comparison between the results of the two different parallel-flow arrangements. It is worth mentioning that many other turbocharger combinations have also been considered, however, the nine combinations analysed produced the best results for the parallel-flow setups in the current study. A wide range of combinations over a wide range of compressor pressure ratios have therefore been considered.

3.1. Low-temperature turbine (LTT) results

The results of the low-temperature turbine (LTT) layout are discussed and analysed in this section. A verification process for this cycle case via a comparison to the results by Van der Merwe et al. [20] is presented in Appendix A. As expected, from this verification process it is shown that the updated model in the current study obtains slightly lower power output and thermal efficiency results (due to the more detailed modelling approach in the current study – see Appendix A for further discussion), however, the trends of the effect of the combustion chamber pressure drop over the compressor pressure ratio range remains the same.

The first consideration that is made for the low-temperature turbine (LTT) layout pertains to the most compatible combinations of the layout. This is done via Fig. 11 where the solid lines indicate obtained solution values that are within the allowed gasifier turbine inlet temperature of 1200 K and where the dashed lines indicate solution values where this temperature is exceeded.

From Fig. 11 it is shown that overall, the combination consisting of the GTX4088R (AR = 1.19) with the GBC14-200 produces the best results across the simulated compressor pressure ratio range in terms of the range of compatibility. The G25-550 (AR = 0.92) with the GBC14-200 also produces good values but only up until a compressor pressure ratio of 2. These combinations and their obtained values across the compressor pressure ratio range are summarised as per Table 1. From Table 1, it is shown that the G25-550 (AR = 0.92) combination offers the best performance in terms of thermal efficiency. The power output is excluded from this consideration as the power output does not differ much between combinations due to being governed by the same power turbine, when comparing the same compressor pressure ratio. However, even though the thermal efficiency is better for the G25-550 (AR = 0.92) combination, this combination is only operational up to a compressor pressure ratio of 2 for the simulated compressor pressure ratios. Thus, the GTX4088R (AR = 1.19) combination is better in terms of the operational range but performs much worse in terms of the cycle thermal efficiency. However, this combination is still discussed in a further analysis, for different combustion chamber pressure loss percentages, in Appendix B, due to the superior compatibility of the combination.

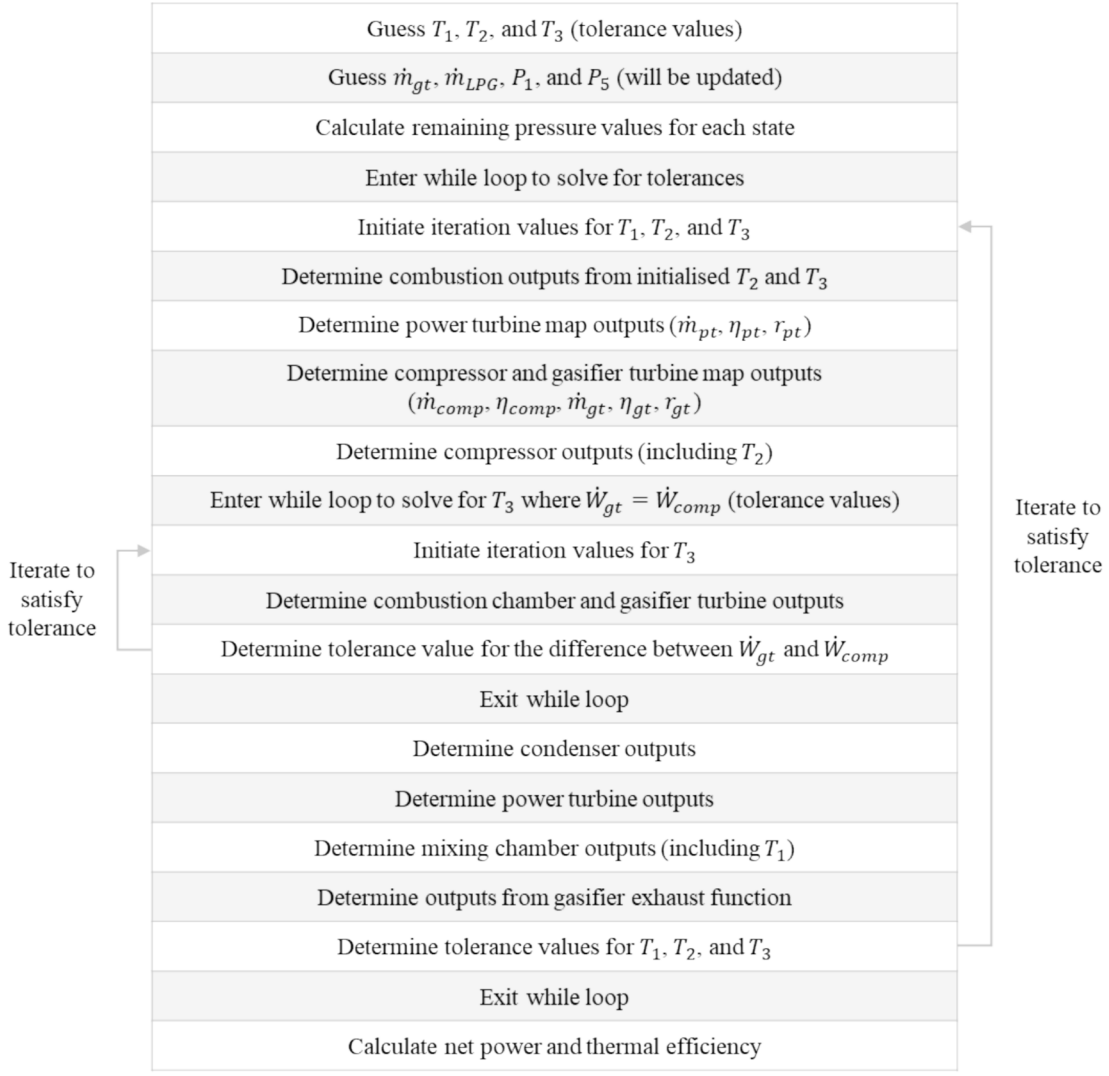

Fig. 10. Turbine inlet air cooling (TIAC) cycle solution procedure.

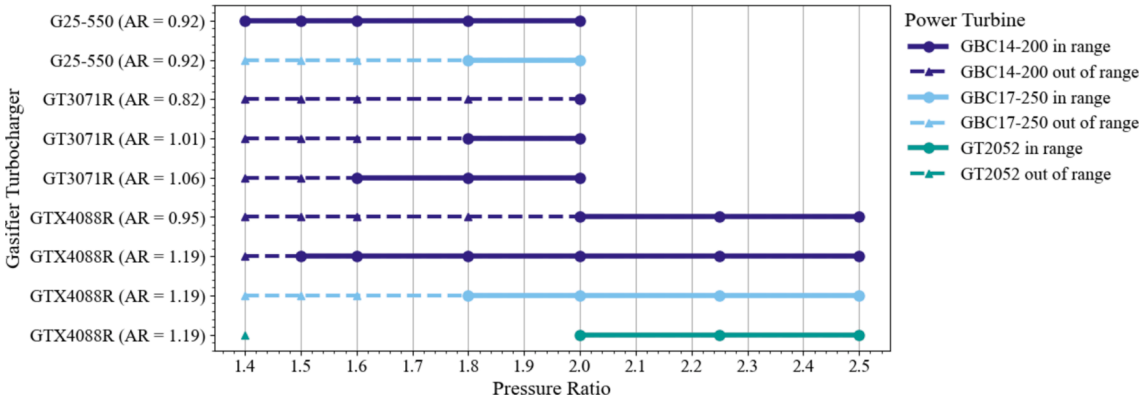

Fig. 11. Low-temperature turbine (LTT) turbocharger compatibility results and compressor pressure ratio ranges at a combustion chamber pressure drop of 6%.

3.2. Turbine inlet air cooling (TIAC) results

For the turbine inlet air cooling (TIAC) layout, the compatibility chart in Fig. 12 illustrates the operational solution ranges for nine different turbocharger combinations under the consideration of a combustion chamber pressure drop of 6 %. As with the low-temperature turbine (LTT) results analysis, the solid lines indicate solution points that are within the allowable maximum gasifier turbine inlet temperature, with the dashed lines indicating compressor pressure ratios where solutions have been found but that are not within the allowable temperature. From Fig. 12, it is clearly observed that both the G25-550 (AR = 0.92) with the GBC14-200 and the GTX4088R (AR = 1.19) with the

Table 1
Comparison between heat input from combustion chamber, power output, and thermal efficiency for different turbochargers with the GBC14-200 as the power turbine for the low-temperature turbine (LTT) cycle setup at a combustion chamber pressure drop of 6%.

Combination	Compressor Pressure Ratio[-]	GT Inlet Temperature [K]	Heat Input [kW]	Power Output [kW]	Thermal Efficiency [%]
G25-550 (AR = 0.92)	1.4	1110	74.8	0.944	1.26
	1.5	1060	79.7	1.298	1.63
	1.6	1044	87.0	1.700	1.95
	1.8	1016	100.1	2.578	2.58
	2.0	1021	114.3	3.446	3.02
	2.25	–	–	–	–
	2.5	–	–	–	–
GTX4088R (AR = 1.19)	1.4	1261	130.8	0.950	0.73
	1.5	1175	137.6	1.306	0.95
	1.6	1133	147.6	1.708	1.16
	1.8	1070	165.8	2.583	1.56
	2.0	1045	184.8	3.444	1.86
	2.25	1066	211.9	4.743	2.24
	2.5	1082	236.3	6.009	2.54

GBC14-200 combinations are fully compatible and within the allowable maximum turbine inlet temperature for the TIAC layout. Thus, these combinations are directly compared in Table 2 for a combustion chamber pressure drop of 6 % under the use of the same condenser geometries.

From Table 2 it is again observed that the G25-550 (AR = 0.92) combination produces better thermal efficiency results. However, under the consideration of the tabulated condenser tube outer diameter and amount of condenser tubes it is shown that the GTX4088 (AR = 1.19) combination produces better compatibility results. This is observed because the G25-550 (AR = 0.92) combination does not have results for this condenser geometry at a compressor pressure ratio of 2.5. Thus, for further results comparison, the GTX4088R (AR = 1.19) combination is discussed while using 45 condenser tubes with an outer diameter of 10 mm. These dimensions are considered as these geometry conditions result in the greatest amount of cooling to the cycle inlet as observed in Fig. 13.

From Fig. 13(a) it is shown that a 10 mm tube diameter results in the most cooling at high compressor pressure ratios, with the 8 mm tube diameter resulting in the best cooling at low compressor pressure ratios. Fig. 13(b) shows that a greater amount of cooling is achieved as the number of tubes increases. When too few tubes are considered, the inlet is heated and not cooled as indicated by the negative heat transfer rate for 15 tubes. In addition to this, the best condenser geometries for cooling also result in the highest outlet water temperatures for domestic heating. The outlet temperature increases as the compressor pressure ratio increases, as observed in Fig. 14. Via Fig. 14(b), it is shown that when 45 condenser tubes are used with a condenser tube outer diameter of 10 mm, at a pressure ratio of 2.5, the water outlet temperature is 324 K (51 °C). This is higher than the specified 38 °C to 42 °C domestic outlet temperature requirement in section 2.2.3. For this geometry, a hot water outlet temperature of 42 °C is obtained at a pressure ratio of approximately 2.1. This implies that the cycle can meet the requirements for the required domestic hot water temperature if the cycle is operated at the correct pressure ratio. The pressure ratio can also be adapted to account for heat loss to the end user. The pressure ratio and condenser geometry can also be changed to achieve a balance between the required hot water temperature and the desired power output (to be discussed further in section 3.3).

The influence of the diameter of the condenser tubes is observed in Figs. 15–18(a). In Fig. 15(a) it is observed that the 8 mm and the 10 mm tubes result in the lowest gasifier turbine inlet temperatures. This is closely linked with a slightly lower combustion heat requirement as observed in Fig. 16(a). This combustion heat increases almost linearly with an increase in the compressor pressure ratio.

From Fig. 17(a) and Fig. 18(a) it is shown that the tube diameters associated with the lowest compressor inlet heating actually result in the best power output and thermal efficiency values, respectively. This is due to the nature of the parallel-flow layout in this study and the influence that cooling the compressor inlet has on the temperature of the power turbine inlet. This power turbine inlet temperature has a subsequent influence on the power output and the thermal efficiency of the cycle, with the thermal efficiency being a function of the power output. Additionally, the power output and thermal efficiency both increase as the compressor pressure ratio increases as in the LTT layout. Higher power outputs and thermal efficiencies are desirable in the operation of the cycle. Thus, it may be more desirable to select poorer performing

Table 2
Comparison between heat input from combustion chamber, power output, and thermal efficiency for different turbochargers with the GBC14-200 as the power turbine for the turbine inlet air cooling (TIAC) setup with a condenser tube diameter of 10 mm and with 45 condenser tubes.

Combination	Compressor Pressure Ratio[-]	GT Inlet Temperature [K]	Heat Input [kW]	Power Output [kW]	Thermal Efficiency [%]
G25-550 (AR = 0.92)	1.5	1038	78.5	1.110	1.41
	1.75	999	95.3	1.928	2.02
	2.0	1004	113.0	2.796	2.47
	2.25	1034	131.9	3.805	2.88
	2.5	–	–	–	–
GTX4088R (AR = 1.19)	1.5	1152	135.5	1.120	0.83
	1.75	1057	158.2	1.935	1.22
	2.0	1030	182.7	2.803	1.53
	2.25	1053	209.8	3.806	1.81
	2.5	1073	234.6	4.789	2.04

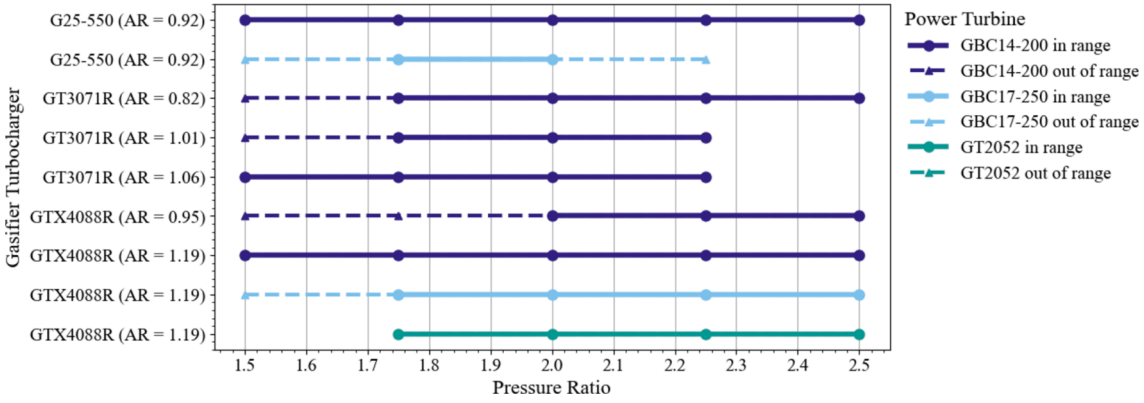

Fig. 12. Turbine inlet air cooling (TIAC) turbocharger compatibility results and compressor pressure ratio ranges at a combustion chamber pressure drop of 6%.

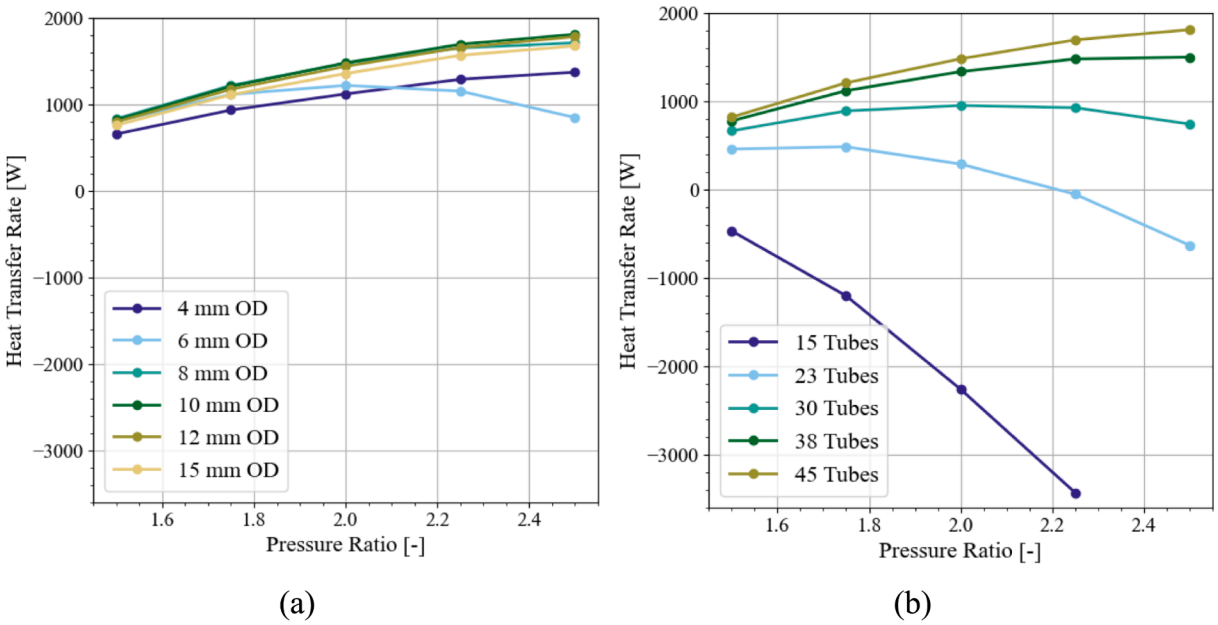

Fig. 13. Mixing chamber heat transfer rate as a function of compressor pressure ratio for the TIAC setup with the GTX4088R (AR = 1.19) as the GT and the GBC14-200 as the PT for (a) different condenser tube outer diameters considering 45 condenser tubes and (b) different amounts of condenser tubes considering a condenser tube outer diameter of 10 mm.

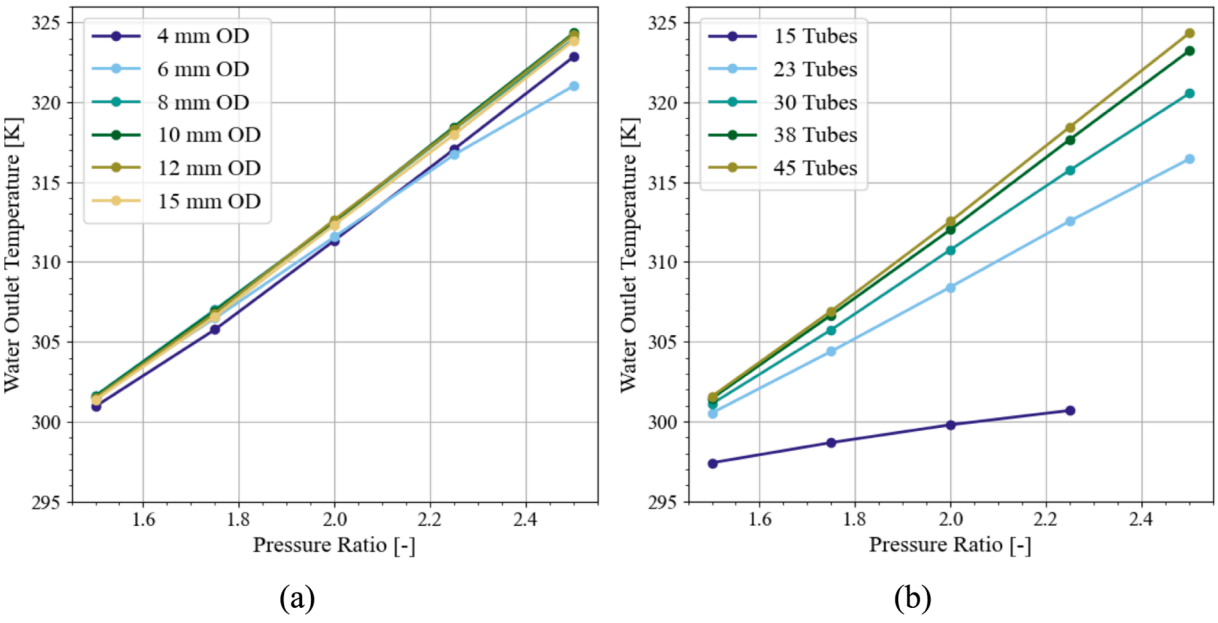

Fig. 14. Condenser water outlet temperature as a function of compressor pressure for the TIAC setup with the GTX4088R (AR = 1.19) as the GT and the GBC14-200 as the PT for (a) different condenser tube outer diameters considering 45 condenser tubes and (b) different amounts of condenser tubes considering a condenser tube outer diameter of 10 mm.

cooling geometries to improve the power output and thermal efficiencies of the cycle.

For an increase in the number of condenser tubes, the subsequent result is a reduction in the gasifier turbine inlet temperature (as shown in Fig. 15(b)), a reduction in the requirement of heat from the combustion chamber (as shown in Fig. 16(b)), and reductions in the power output and thermal efficiency values (as shown in Fig. 17(b) and Fig. 18(b)). All of these values, with the exception of the gasifier turbine inlet temperature, increase with an increase in the compressor pressure ratio. This shows that the only real cycle improvement, as the number of tubes increases, is the lower reliance on combustion heat and the lower gasifier turbine inlet temperatures. These lower gasifier turbine inlet temperatures allow the layout results to remain within the allowable gasifier turbine inlet temperature of 1200 K.

3.3. Comparison between LTT and TIAC results

Following from an analysis of the results of each cycle layout, the results of the low-temperature turbine (LTT) can be compared to that of the turbine inlet air cooling (TIAC) layout. This is initially done for the combination between the GTX4088R (AR = 1.19) with the GBC14-200 as the combination produces good compatibility results for both cases

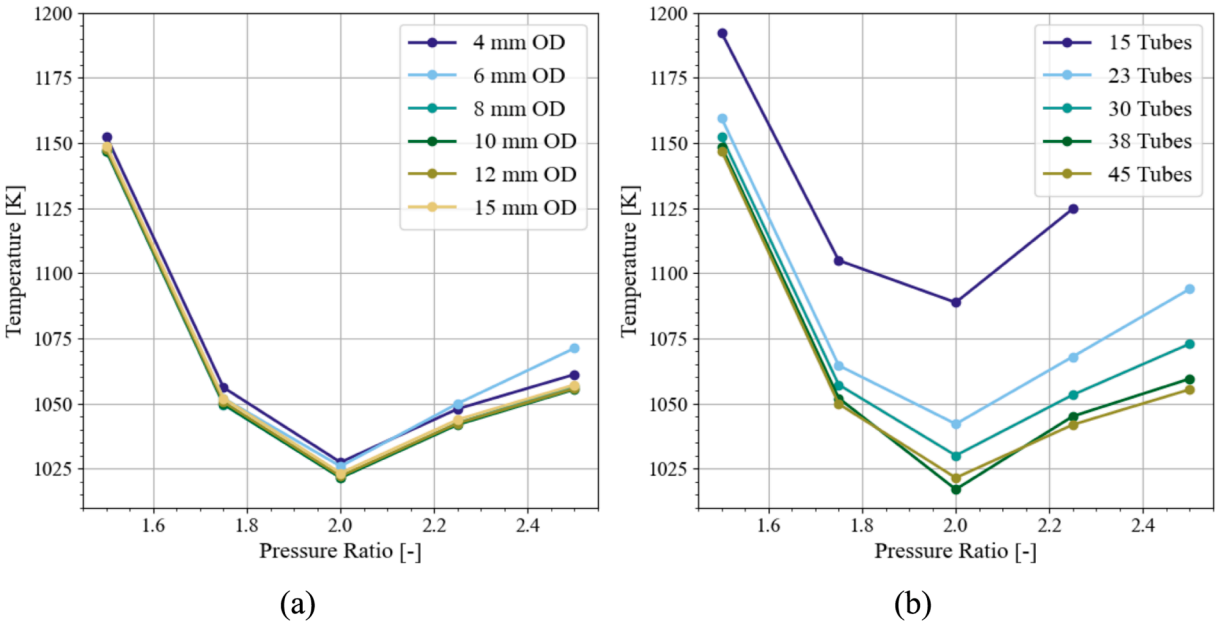

Fig. 15. GT inlet temperature as a function of compressor pressure ratio for the TIAC setup with the GTX4088R (AR = 1.19) as the GT and the GBC14-200 as the PT for (a) different condenser tube outer diameters considering 45 condenser tubes and (b) different amounts of condenser tubes considering a condenser tube outer diameter of 10 mm.

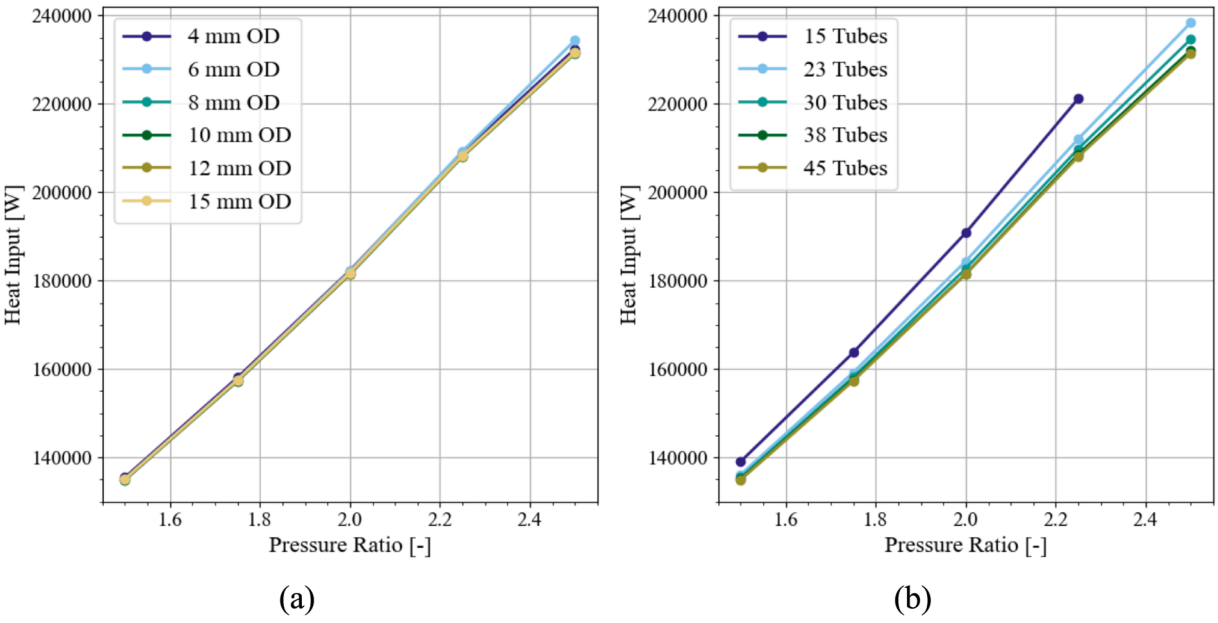

Fig. 16. Combustion heat required as a function of compressor pressure ratio for the TIAC setup with the GTX4088R (AR = 1.19) as the GT and the GBC14-200 as the PT for (a) different condenser tube outer diameters considering 45 condenser tubes and (b) different amounts of condenser tubes considering a condenser tube outer diameter of 10 mm.

at a combustion chamber pressure drop of 6 %. Note that higher power outputs and thermal efficiencies are more beneficial in the operation of the cycles. Thus, even though the TIAC cycle may offer water heating (which is an additional TIAC aspect that the LTT cycle does not offer), the power outputs and thermal efficiencies are of more importance in the analyses of the cycles.

Under the consideration of different condenser tube diameters, it is shown that the TIAC cycle has lower associated gasifier turbine temperatures, as per Fig. 19(a). This allows for these temperatures to be further within the limit of the turbine inlet temperature of 1200 K. In Fig. 20(a) it is shown that this is linked to the lower combustion heat requirement when adequate cooling is applied in the TIAC layout. However, even though lower heat amounts and lower gasifier turbine inlet temperatures are required for the operation of the TIAC cycle in comparison to the LTT cycle, the TIAC layout produces considerably less power output and thermal efficiency, as observed in Fig. 21(a) and Fig. 22(a), when compared at the same compressor pressure ratio. This is due to the consequential cooling of the power turbine inlet in the TIAC setup. This is greatly as a result of the TIAC cycle having a lower inlet temperature to the power turbine (as dictated by the outlet air temperature of the condenser when enough cooling is applied to the cycle). This lower power turbine inlet temperature results in a slightly higher

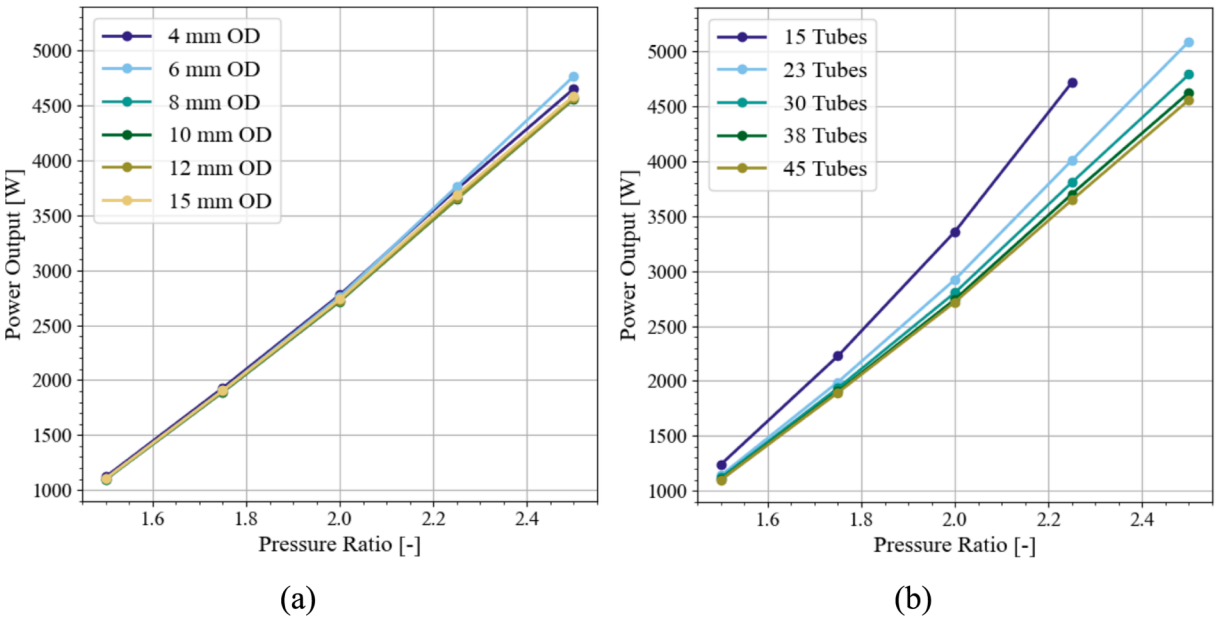

Fig. 17. Net power output as a function of compressor pressure ratio for the TIAC setup with the GTX4088R (AR = 1.19) as the GT and the GBC14-200 as the PT for (a) different condenser tube outer diameters considering 45 condenser tubes and (b) different amounts of condenser tubes considering a condenser tube outer diameter of 10 mm.

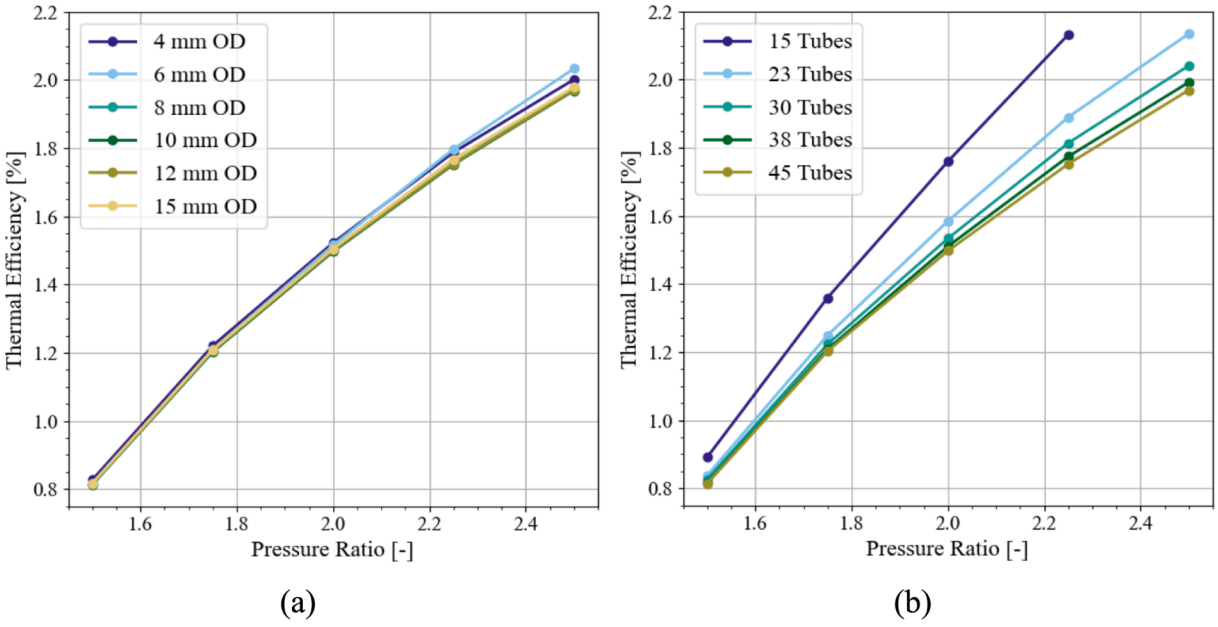

Fig. 18. Thermal efficiency as a function of compressor pressure ratio for the TIAC setup with the GTX4088R (AR = 1.19) as the GT and the GBC14-200 as the PT for (a) different condenser tube outer diameters considering 45 condenser tubes and (b) different amounts of condenser tubes considering a condenser tube outer diameter of 10 mm.

power turbine mass flow rate in proportion to the LTT cycle when condenser geometries are used that result in lower amounts of cooling. This is determined based on the turbomachinery flow map relations in section 2.2.1.

A higher power turbine mass flow rate results in a greater amount of power generation in the power turbine. However, due to the reduced inlet temperature to the power turbine having a greater influence on the power output performance of the cycle, there is a reduction of power output in the cooled TIAC cycles. This is observed to influence the power output results in Fig. 21(a). This lower power output results in lower thermal efficiency, as observed in Fig. 22(a), with the combustion heat reduction in Fig. 19(a) not being enough to allow for higher thermal efficiencies in the TIAC cycle.

Similar results are shown in Fig. 19(b) to Fig. 22(b) for differing amounts of condenser tubes in comparison to differing condenser tube diameters. However, it is shown that when too few condenser tubes are used, and when additional heat is applied to the compressor inlet as a result, the gasifier turbine inlet temperatures and the combustion heat increase. In these instances, the power output and thermal efficiency values are still lower in the TIAC cycle when compared to the LTT cycle. This is due to a mass flow rate shift in the power turbine of the cycle and its subsequent influence on the power output of the cycle. The thermal

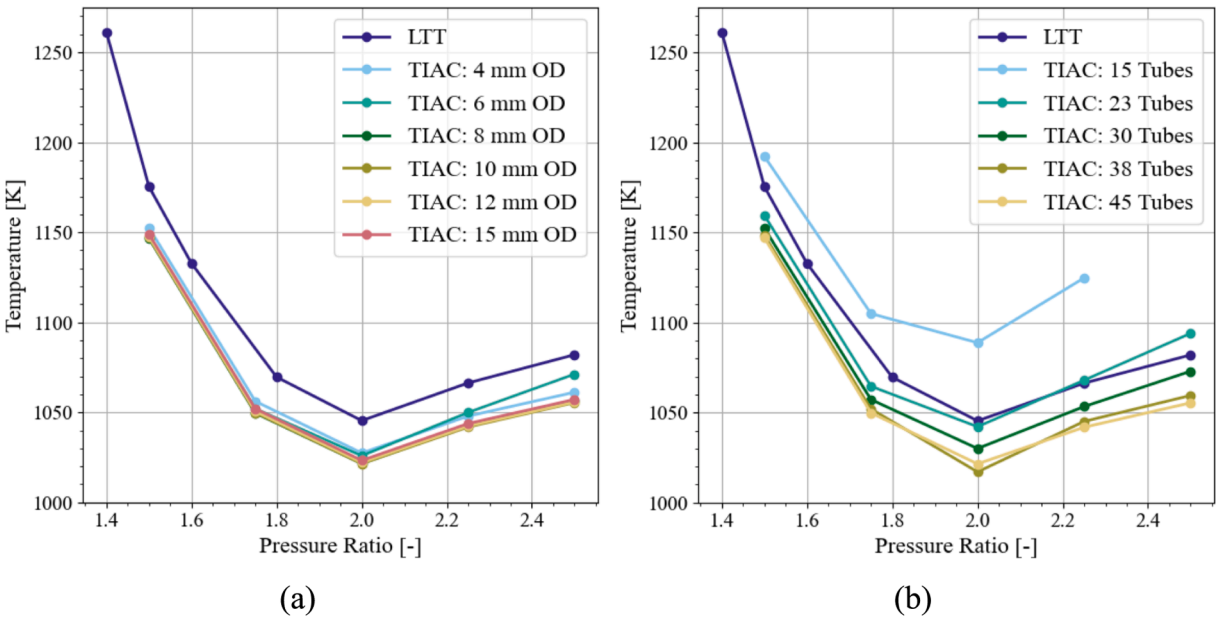

Fig. 19. GT inlet temperature as a function of compressor pressure ratio for the LTT and TIAC setups with the GTX4088R (AR = 1.19) as the GT and the GBC14-200 as the PT for (a) different condenser tube outer diameters considering 45 condenser tubes and (b) different amounts of condenser tubes considering a condenser tube outer diameter of 10 mm.

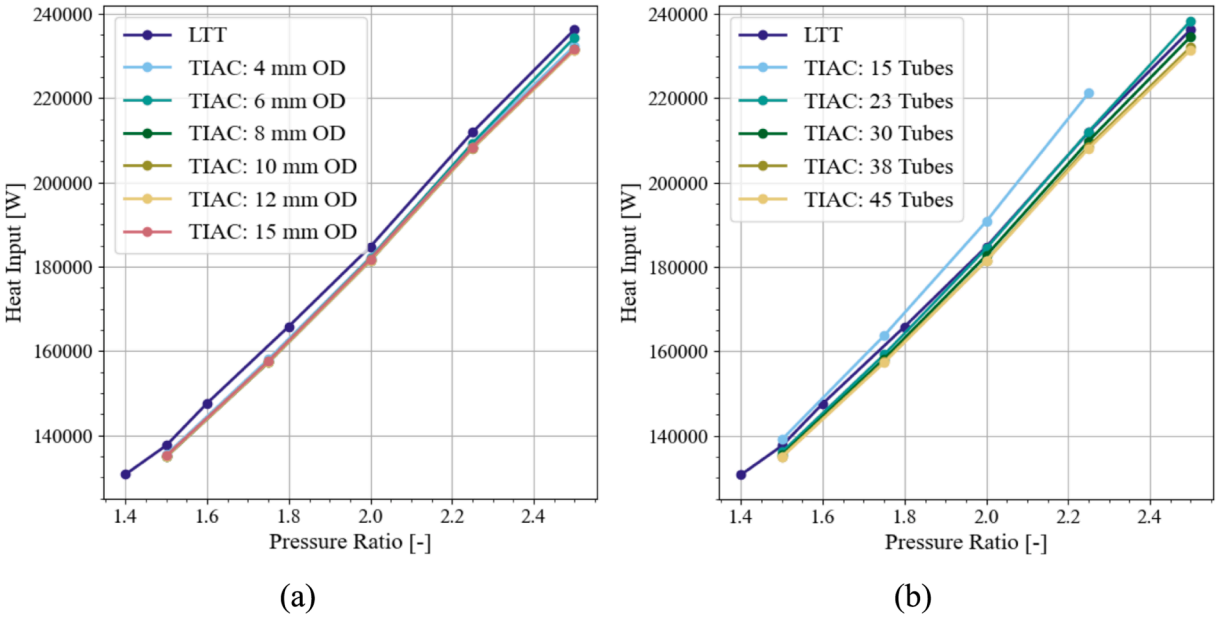

Fig. 20. Combustion heat required as a function of compressor pressure ratio for the LTT and TIAC setups with the GTX4088R (AR = 1.19) as the GT and the GBC14-200 as the PT for (a) different condenser tube outer diameters considering 45 condenser tubes and (b) different amounts of condenser tubes considering a condenser tube outer diameter of 10 mm.

efficiency decreases due to lower power output with a greater combustion heating requirement when cooling is not applied to the compressor inlet in the TIAC cycle.

Moreover, the insertion of the cooling cycle components extends the operational compressor pressure ratio range of the cycle and, in some instances, may allow for better output performance results. This is due to operation at compressor pressure ratios where results have not been obtained or where the gasifier turbine inlet temperature exceeds 1200 K. This is visually observed in Fig. 23 to Fig. 24, where, for a comparison between the layouts for the G25-550 (AR = 0.92) and GBC14-200 combination, it is shown that even though the power output and thermal efficiency is lower for the TIAC cycle at the same compressor pressure ratio, higher power output and thermal efficiency values can be obtained. This is due to the ability of the TIAC cycle to operate at greater compressor pressure ratios. This performance improvement is further quantified through Table 3 where the TIAC cycle produces better power output and thermal efficiency results, but with a higher heating requirement due to the higher compressor pressure ratio of operation.

Furthermore, it is shown in Fig. 25 that the compressor work in the TIAC cycle is slightly lower for geometries associated with cooling the compressor inlet. That is, when enough condenser tubes are used for cooling, the compressor work is slightly less than in the LTT layout.

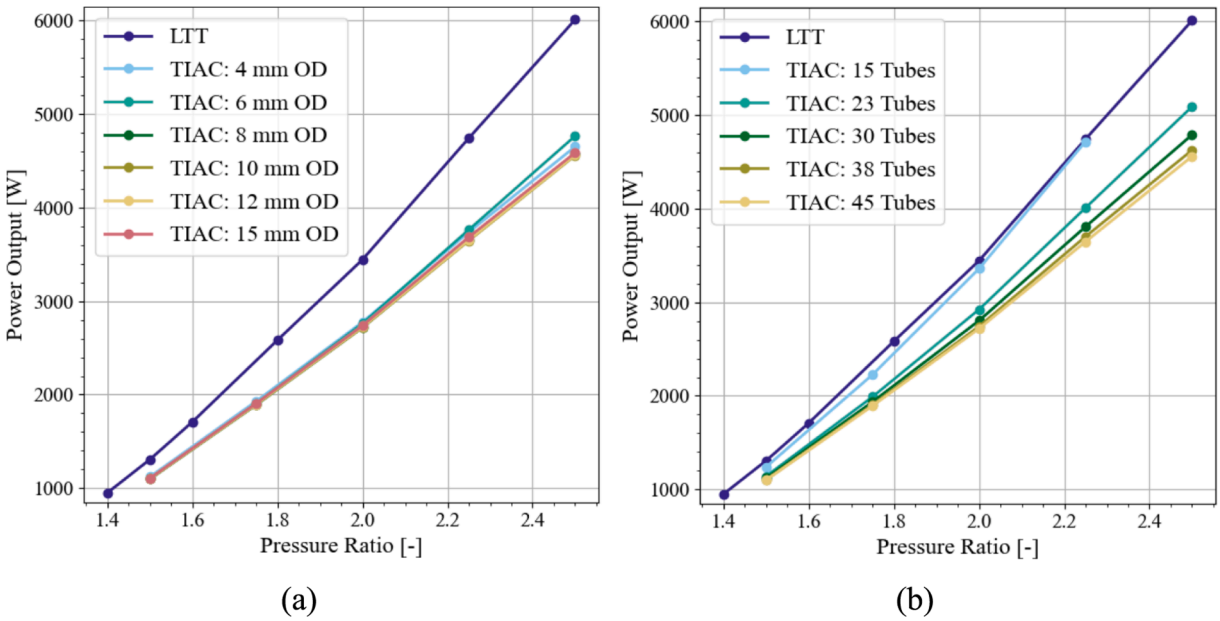

Fig. 21. Net power output as a function of compressor pressure ratio for the LTT and TIAC setups with the GTX4088R (AR = 1.19) as the GT and the GBC14-200 as the PT for (a) different condenser tube outer diameters considering 45 condenser tubes and (b) different amounts of condenser tubes considering a condenser tube outer diameter of 10 mm.

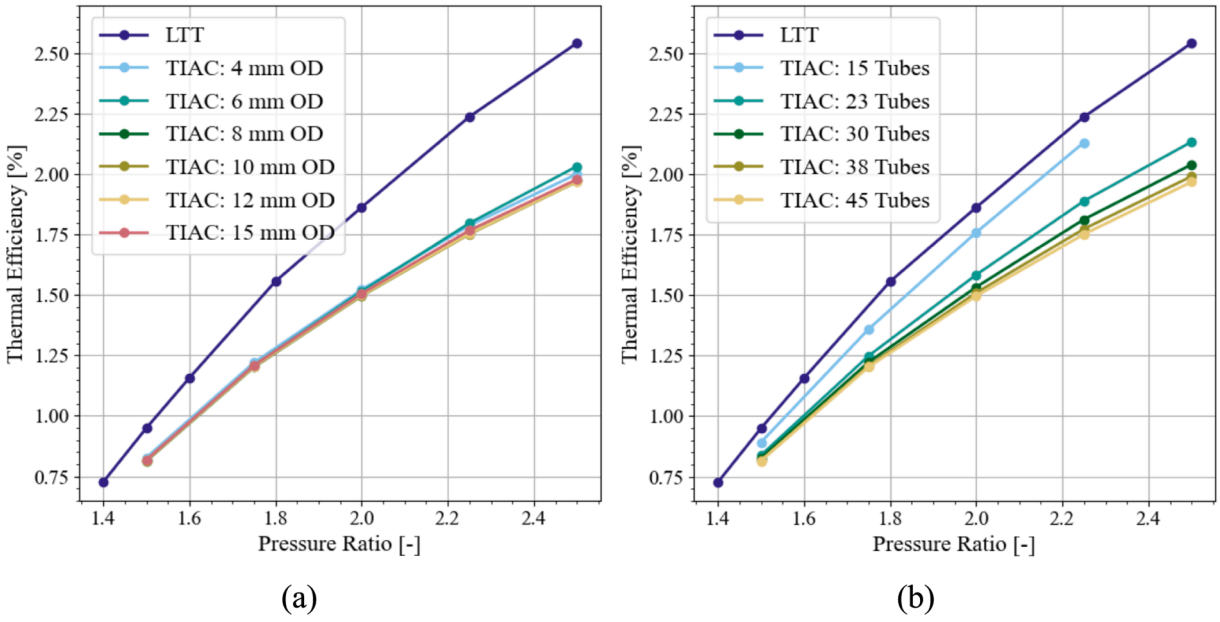

Fig. 22. Thermal efficiency as a function of compressor pressure ratio for the LTT and TIAC setups with the GTX4088R (AR = 1.19) as the GT and the GBC14-200 as the PT for (a) different condenser tube outer diameters considering 45 condenser tubes and (b) different amounts of condenser tubes considering a condenser tube outer diameter of 10 mm.

When too few tubes are used, the compressor inlet is heated, and more compressor power is required to operate the cycle. There are only slight differences in this consideration which indicates that the TIAC cycle does slightly reduce the required compressor power but due to the limited cooling to the compressor inlet, the cooling effect is not enough to significantly lower the compressor power. This is important to consider because the purpose of TIAC is to reduce the inlet temperature to the compressor to improve the efficiency of the compressor so that the turbines do not need to supplement as much of the required power to the compressor (as per Ref. [12]). This is, however, not seen in Fig. 25 as it is shown that there is a minimal influence of the cooling values on the compressor inlet and thus the provided TIAC cycle inlet cooling is not enough to sufficiently lower the required compressor power. This cooling effect does however have a greater influence at higher pressure ratios.

In summary of a comparison between the LTT and the TIAC cycles, the TIAC cycle mostly cannot offer better power output nor thermal efficiency than the LTT cycle when the GTX4088R (AR = 1.19) is used as the main shaft turbocharger with the GBC14-200 as the power turbine. However, due to the ability of the TIAC cycle to operate at a higher pressure ratio when the G25-550 (AR = 0.92) is used as the main shaft turbocharger with the GBC14-200 as the power turbine, the TIAC cycle

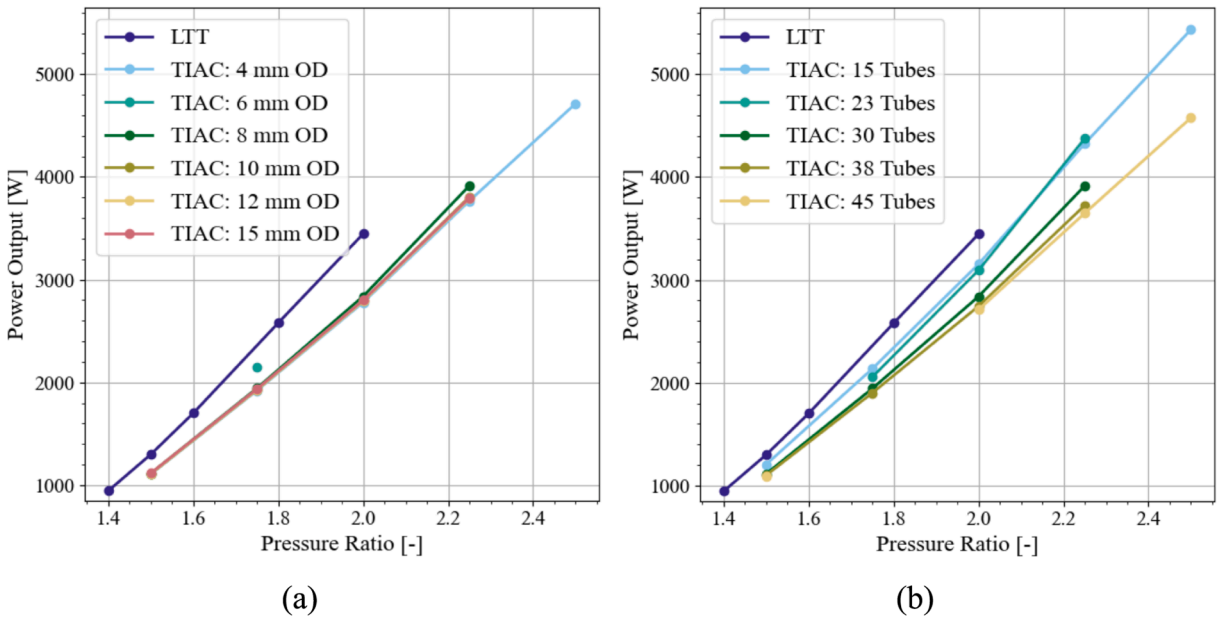

Fig. 23. Net power output as a function of compressor pressure ratio for the LTT and TIAC setups with the G25-550 (AR = 0.92) as the GT and the GBC14-200 as the PT for (a) different condenser tube outer diameters considering 30 condenser tubes and (b) different amounts of condenser tubes considering a condenser tube outer diameter of 8 mm.

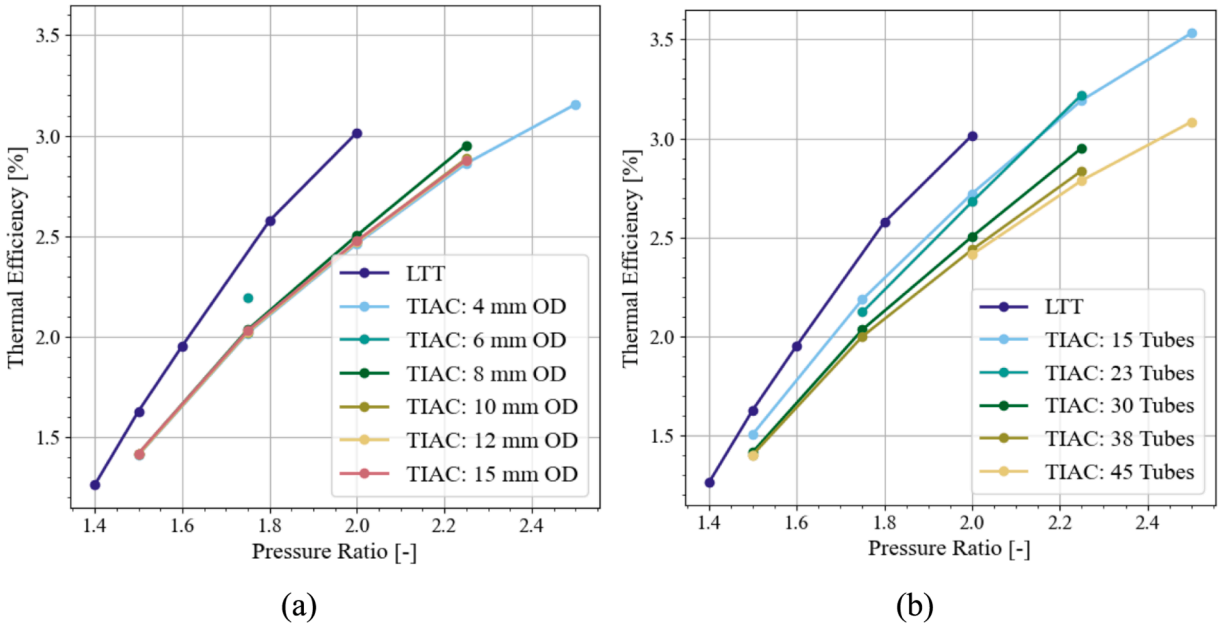

Fig. 24. Thermal efficiency as a function of compressor pressure ratio for the LTT and TIAC setups with the G25-550 (AR = 0.92) as the GT and the GBC14-200 as the PT for (a) different condenser tube outer diameters considering 30 condenser tubes and (b) different amounts of condenser tubes considering a condenser tube outer diameter of 8 mm.

is able to obtain overall better power output and thermal efficiency than the LTT cycle at the optimum pressure ratio of each cycle. When 45 condenser tubes with tube outer diameters of 8 mm are used, the TIAC cycle is capable of providing 38.8 °C (311.9 K) to 50.7 °C (323.8 K) of hot outlet water (as per Fig. 26) between pressure ratios of 2 and 2.5 (where the LTT cycle does not obtain any values). This occurs while obtaining power outputs of between 2.7 kW and 4.6 kW (see Fig. 23), and thermal efficiencies of between 2.4 % and 3.1 % (see Fig. 24), for the same pressure ratio range. The higher power output, thermal efficiency, and water outlet temperature values occur at a pressure ratio of 2.5. This shows that the TIAC cycle can offer better performance than the LTT cycle while also producing hot water for domestic use.

Lastly, the TIAC and LTT cycles can be compared to the cycle concept by Zaki et al. [19]. The Zaki et al. [19] cycle makes use of a generator coupled to the main shaft of the cycle with additional power generated from the power turbine using another generator. Appendix C shows an investigation similar to the main TIAC cycle in this study, with the utilisation of the basic Zaki layout, and shows that the cycle offers better performance when the generator is not only coupled to the power turbine, but with an additional generator coupled to the main shaft turbocharger. This is due to the gasifier turbine inlet temperature of the basic Zaki layout being at its maximum of 1200 K while using the

Table 3
Direct comparison between conditions for maximum thermal efficiency obtained through the simulation of the LTT and the TIAC setups for a combustion chamber pressure drop of 6 % for the G25-550 (AR = 0.92) as the main shaft turbocharger and with the GBC14-200 as the power turbine.

Parameter	LTT	TIAC	Difference [%]
Pressure Ratio [-]	2.0	2.5	25.00
Condenser Tube Diameter [mm]	–	12	–
Number of Tubes [-]	–	15	–
Heat Input [kW]	114.25	150.08	31.36
Power Output [kW]	3.446	5.682	64.89
Thermal Efficiency [%]	3.02	3.65	20.86
GT Inlet Temperature [K]	1021	1120	9.70

gasifier turbine power output to power the compressor. The net power output is from the power turbine as well as the remaining power from the gasifier turbine's shaft. This is however a more expensive cycle to manufacture due to the usage of two generators. Additionally, due to space restrictions, it is more difficult to couple a generator to the main shaft turbocharger.

3.4. Exergy analysis and cycle feasibility

To analyse the cycles in terms of exergy analysis the irreversibility rates of the components in the LTT and TIAC cycles can be summarised as per Fig. 27 and Fig. 28, respectively. Each of these figures are generated for a pressure ratio of 2, as a good performing, mid-range pressure ratio. Fig. 28 is generated based on 45 condenser tubes and a tube outer diameter of 10 mm as these geometries allow for the highest cooling heat transfer rate at this pressure ratio.

The TIAC cycle allows for a slight reduction in the total cycle irreversibility and slight reductions in the irreversibility rates of some of the cycle components. These reductions can be observed through comparing Fig. 27 and Fig. 28 to one another. The TIAC cycle has the greatest influence on the irreversibility rate of the gasifier turbine exhaust, which is the greatest source of irreversibility in both the LTT and the TIAC cycle. The power turbine irreversibility completely falls away as a direct result of the power turbine no longer exhausting to the atmosphere. Thus, the addition of cooling in the TIAC cycle does not reduce the cycle component irreversibility rates significantly but the irreversibility rates of the exhaust processes are reduced.

4. Conclusion and recommendations

4.1. Conclusion

In conclusion, this study forms a comparison between a low-temperature turbine (LTT) parallel-flow Brayton cycle and a similar parallel-flow cycle with the inclusion of turbine inlet air cooling (TIAC) through a consideration of different geometries for the condenser in the cooling cycle section to ascertain which cycle offers the best power output and thermal efficiency results. Results show that:

- The TIAC cycle, with a sufficient amount of cooling, successfully reduces the required gasifier turbine inlet temperature in comparison to the results of the LTT cycle. This is important due to the turbocharger manufacturer limits for this temperature.
- There is a shift of the optimum operating point in the TIAC cycle which allows for a greater operational range that is within the inlet temperature limits of commercial *Garrett Motion* turbochargers and can also result in more power output and thermal efficiency at higher, previously inaccessible, compressor pressure ratios.
- When comparing the LTT and TIAC cycles at the optimum operating point (which shifts to a higher compressor pressure ratio for the TIAC setup), for the G25-550 (AR = 0.92) main shaft turbocharger and the GBC14-200 power turbine, the TIAC layout obtains 64.9 % more power output and a 31.4 % improvement in thermal efficiency.
- There are no power output nor thermal efficiency improvements for the TIAC cycle in comparison to the LTT cycle when using the TIAC cycle with the GTX4088R (AR = 1.19) as the main shaft turbocharger and with the GBC14-200 as the power turbine. This statement holds under a consideration of both optimum and local pressure ratio operating points.
- The TIAC cycle is able to provide enough water heating for domestic use at temperatures between 38 °C and 42 °C and can provide hot water temperatures of up to 51 °C at the highest simulated compressor pressure ratio for both main shaft turbocharger options considered.

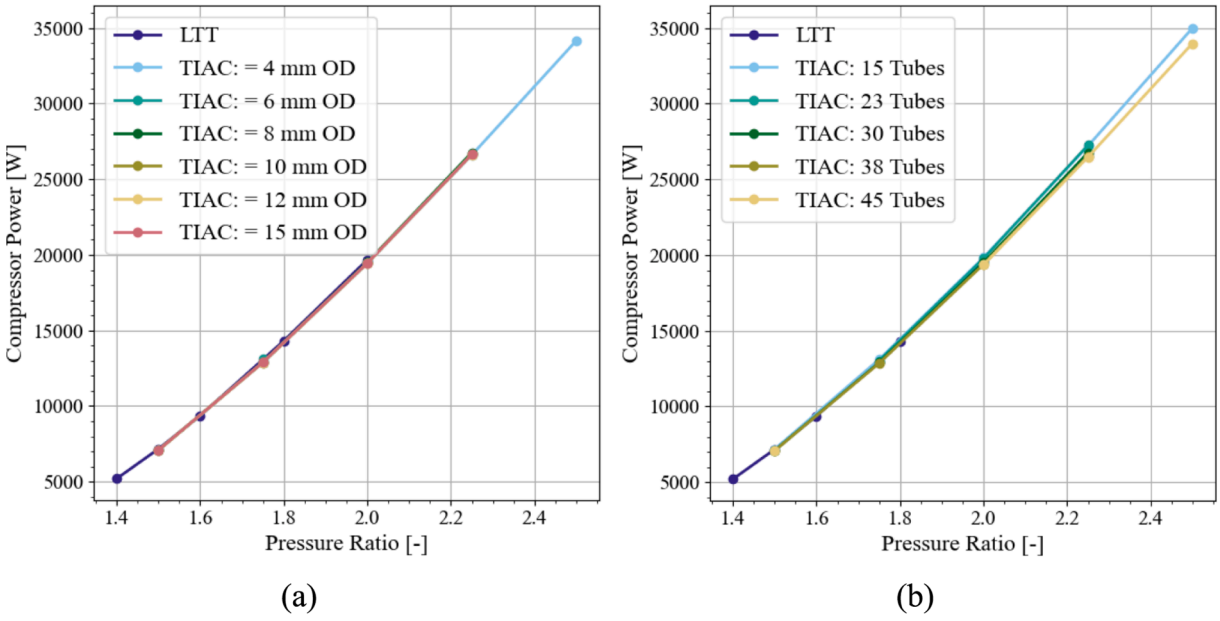

Fig. 25. Compressor power required as a function of compressor pressure ratio for the LTT and TIAC setups with the G25-550 (AR = 0.92) as the GT and the GBC14-200 as the PT for (a) different condenser tube outer diameters considering 30 condenser tubes and (b) different amounts of condenser tubes considering a condenser tube outer diameter of 8 mm.

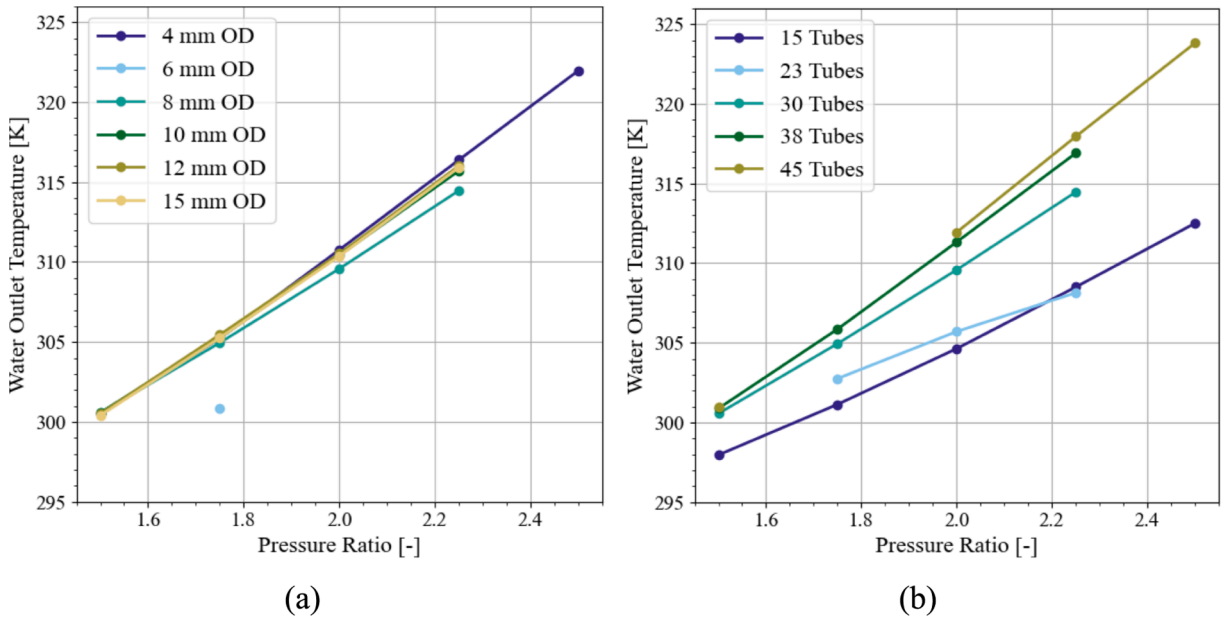

Fig. 26. Condenser water outlet temperature as a function of compressor pressure ratio for the LTT and TIAC setups with the G25-550 (AR = 0.92) as the GT and the GBC14-200 as the PT for (a) different condenser tube outer diameters considering 30 condenser tubes and (b) different amounts of condenser tubes considering a condenser tube outer diameter of 8 mm.

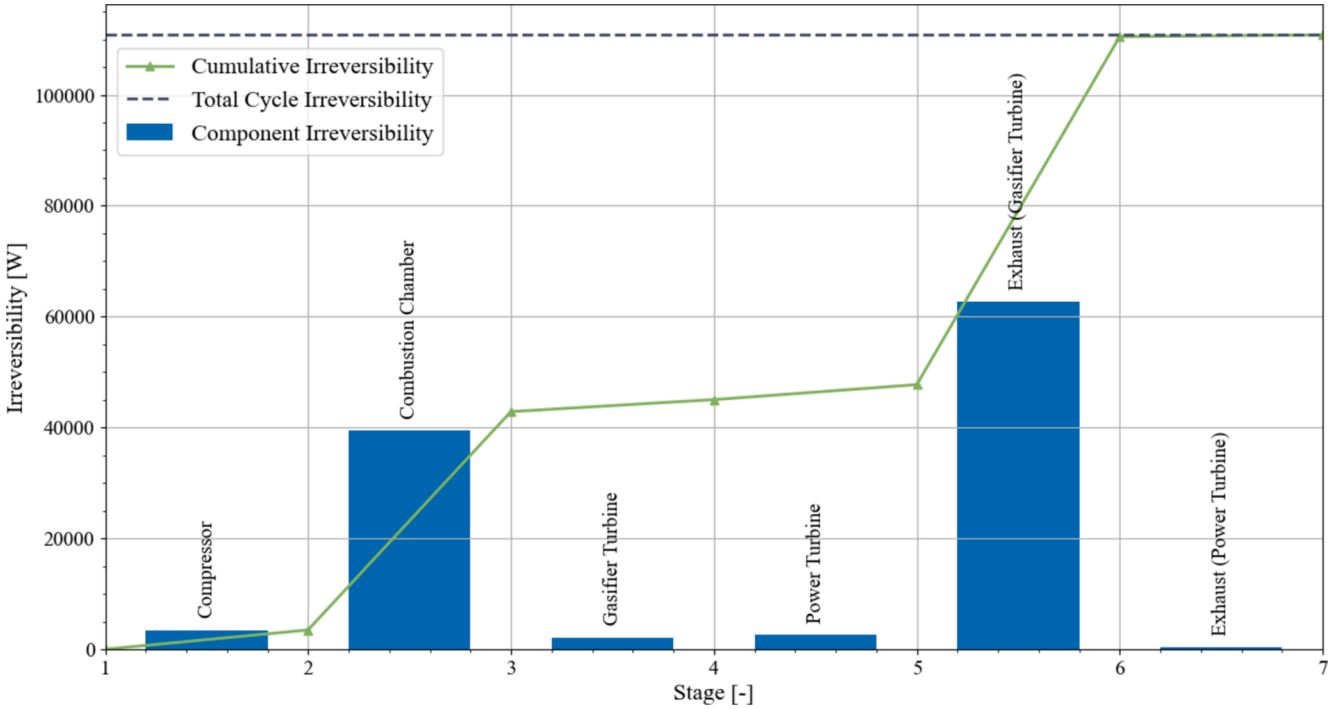

Fig. 27. Cumulative irreversibility through LTT cycle at a compressor pressure ratio of 2 – with the G25-550 (AR = 0.92) as the GT and the GBC14-200 as the PT.

- It is shown that TIAC does not form a viable cycle addition in terms of a power output and thermal efficiency improvement when compared at the same compressor pressure ratio.

4.2. Recommendations

The first recommendation that can be made to develop the study further is the consideration of different cooling component dimensions. For example, more dimensions can be considered for the condenser tube diameters and number of tubes, and an investigation can be pursued to study the influence that different condenser and mixing chamber lengths will have on the results of the TIAC cycle. Moreover, a direct study regarding the usage of the condenser outlet water for domestic use can be further considered in terms of an overall energy utilisation factor as per the procedure by Le Roux [47]. It is also recommended to implement an experimental study pertaining to the cycle layouts in the current study for validation and practical implementation purposes. Lastly, the influence of adding a recuperator or solar heat input to the cycle can be investigated to ascertain the influence of these additions to the cycle's thermal efficiency improvement.

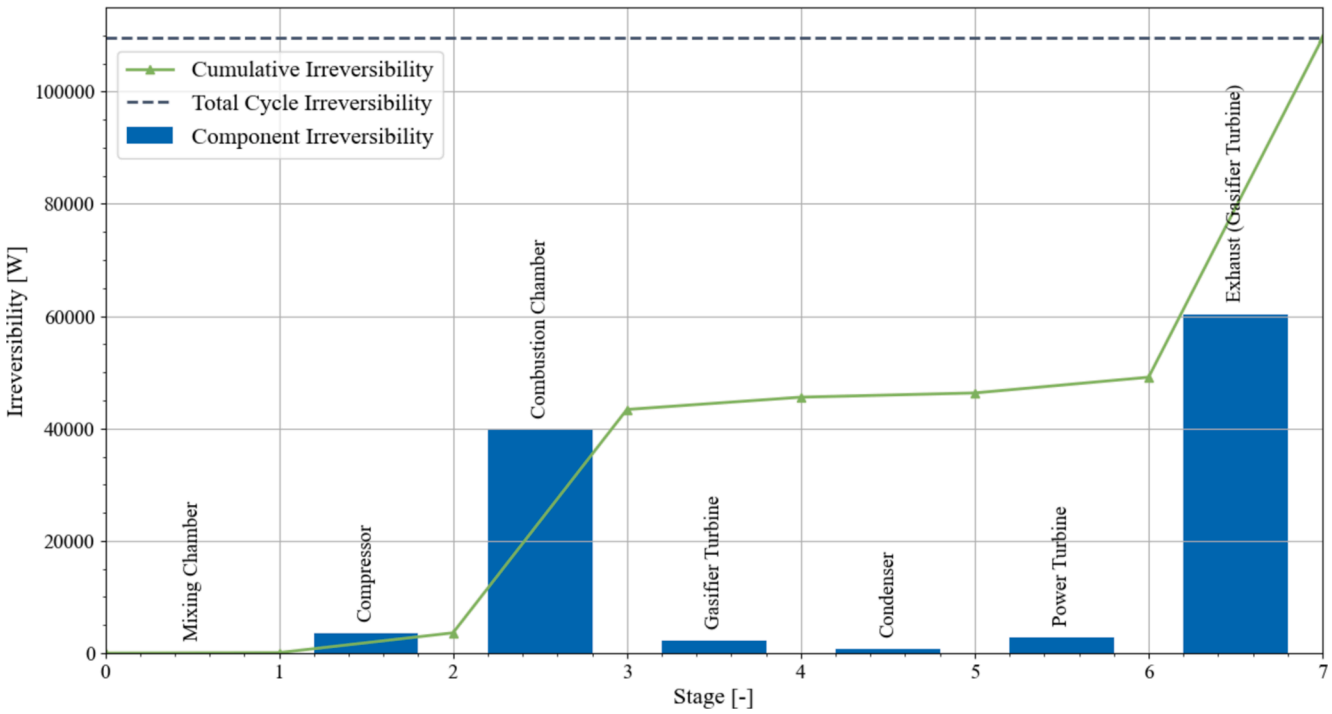

Fig. 28. Cumulative irreversibility through TIAC cycle at a compressor pressure ratio of 2 with 45 condenser tubes with an outer diameter of 10 mm – with the G25-550 (AR = 0.92) as the GT and the GBC14-200 as the PT.

CRediT authorship contribution statement

C.C. Cockcroft: Writing – review & editing, Writing – original draft, Visualization, Validation, Software, Methodology, Investigation, Formal analysis, Data curation, Conceptualization. **W.G. Le Roux:** Writing – review & editing, Writing – original draft, Supervision, Resources, Project administration, Methodology, Funding acquisition, Conceptualization.

Declaration of competing interest

The authors declare that they have no known competing financial interests or personal relationships that could have appeared to influence the work reported in this paper.

Acknowledgements

The authors are grateful for the financial support of the UP Solar Thermal Spoke as provided by the Renewable Energy Hub and Spokes Programme of the Department of Science and Innovation (DSI), South Africa.

Appendix A. Low-temperature turbine (LTT) verification

In the study done by Van der Merwe et al. [20], the LTT setup has been simulated and discussed for a combination between the G25-550 (AR = 0.92) and the GBC14-200. Thus, the results of the current study can be compared to the results by Van der Merwe et al. [20] for the same turbocharger combination. This is done via Fig. A1 for the cycle power output and via Fig. A2 for the thermal efficiency. A combustion chamber pressure drop of up to 4 % has been simulated by Van der Merwe et al. [20], however, the current study simulates a combustion chamber pressure drop of 6 % according to Lefebvre & Ballal [38] for an annular combustion chamber. For a comparison between the current study and the study by Van der Merwe et al. [20], combustion chamber pressure drop values of up to 4 % are considered. It is also noted that the study by Van der Merwe et al. [20] formed an initial analysis of the LTT cycle with various simplifications and limitations. The current study extends on the analysis through incorporating cycle complexities in the form of updated combustion gas properties and the incorporation of the fuel mass flow rate as required for the combustion process.

Note that the maximum turbine efficiency of the GBC14-200 and GBC17-250 was assumed to be 65 % as per the study by Van der Merwe et al. [20]. The maximum efficiency of a turbine in an automotive turbocharger is usually between 65 % and 75 % according to Guzzella & Onder [48] and therefore it is a conservative assumption.

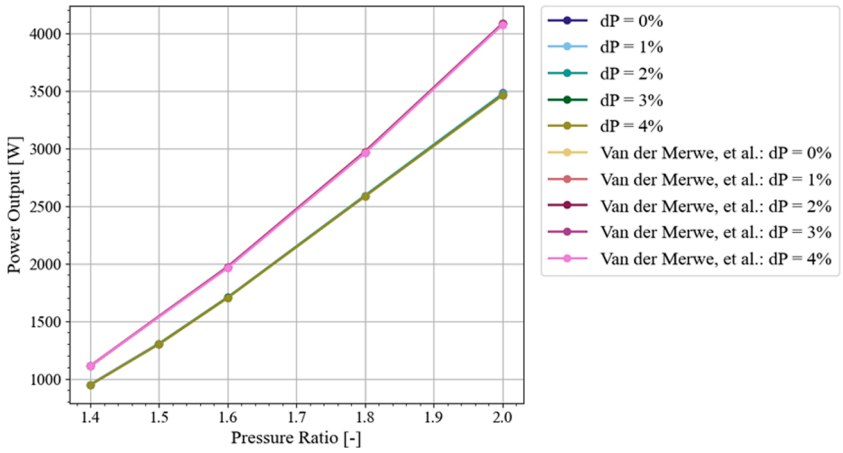

Fig. A1. Comparison between power output values for verification over change in pressure ratio for LTT setup with the G25-550 (AR = 0.92) as the GT and the GBC14-200 as the PT

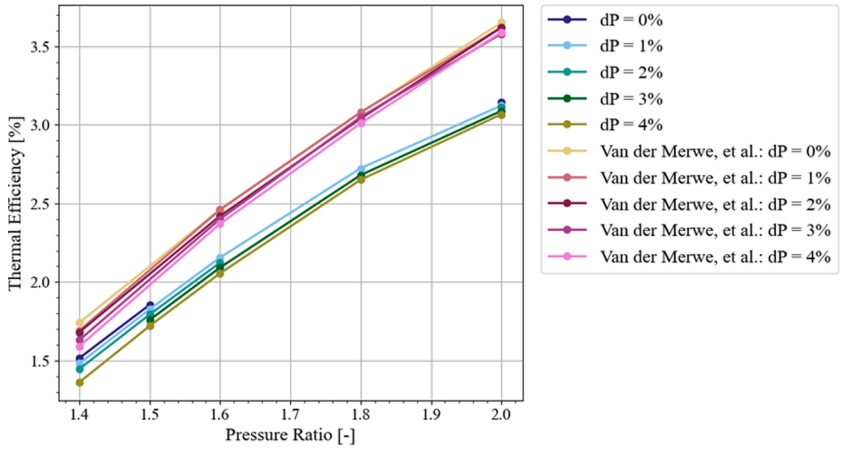

Fig. A2. Comparison between thermal efficiency values for verification over change in pressure ratio for LTT setup with the G25-550 (AR = 0.92) as the GT and the GBC14-200 as the PT

From Figs. A1 and A2 it is observed that the trends of the two studies are similar. An increase in both the thermal efficiency and power output is observed as the compressor pressure ratio increases, with a negligible deviation in the power output as the combustion chamber pressure drop increases, and with a reduction in the thermal efficiency of the cycle as the combustion chamber pressure drop increases. However, it is shown in Figs. A1 and A2 that the cycle performance in the current study is lower than that of the study by Van der Merwe et al. [20]. This is due to slightly different modelling procedures as discussed below.

The first modelling procedure in this study that can result in different cycle performance is the manner in which values are obtained from the turbomachinery contour maps. The current study applies a contour plot to the compressor map and obtains the map values through interpolation from contour lines, whereas Van der Merwe et al. [20] obtained results via the placement of a fine mesh over the map data and an interpolation from this fine mesh. Additionally, the current study uses a more realistic combustion model that accounts for the mass flow rate of the fuel injected into the cycle. The reference study considers a heating process instead of a combustion process and subsequently does not include the fuel mass flow rate. An additional modelling deviation persists in the fact that the current study minimises the reliance on ideal gas assumptions in comparison to the reference study and does not model the combustion products as air but rather using an appropriate air–fuel mixture model. All of these deviations can result in different power output and thermal efficiency values for the cycles as observed in Figs. A1 and A2.

Appendix B. Low-temperature turbine (LTT) results with change in combustion pressure loss

To ascertain the influence of the combustion chamber pressure drop on the results of the LTT layout, the cycle is simulated for the combination between the GTX4088R (AR = 1.19) and the GBC14-200 as an example solution set considering different pressure drop percentages. The results of this analysis are shown in Fig. B1 to Fig. B4.

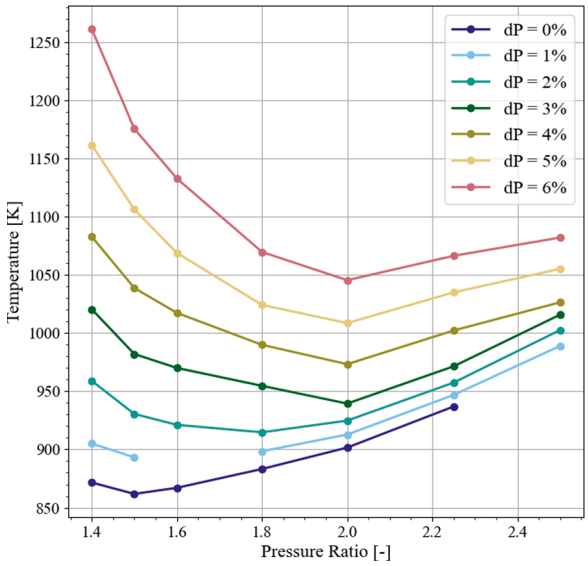

Fig. B1. GT inlet temperature as a function of compressor pressure ratio for different combustion chamber pressure drop percentages – for the LTT setup with the GTX4088R (AR = 1.19) as the GT and the GBC14-200 as the PT

From Fig. B1 it is shown that the gasifier turbine inlet temperature increases with an increase in the combustion chamber pressure drop. This is due to an increased pressure drop resulting in a lower gasifier turbine pressure ratio as the cycle needs to exhaust at the ambient pressure regardless of the combustion chamber pressure drop. This means that more heat needs to be supplied at higher pressure drop percentages, as seen in Fig. B2, to increase the gasifier turbine inlet temperature so that the compressor and gasifier turbine power amounts balance out. Additionally, the profile of the gasifier turbine inlet temperature follows a non-linear trend over a change in the compressor pressure ratio due to the non-linear compressor flow maps. This is shown where the inlet temperature obtains a turning point in regions where it is assumed the compressor pressure ratio results in better compressor efficiency values and a lower requirement for gasifier turbine power generation. This turning point shifts as the combustion chamber pressure drop changes due to the coupled nature of the compressor and gasifier turbine turbomachinery.

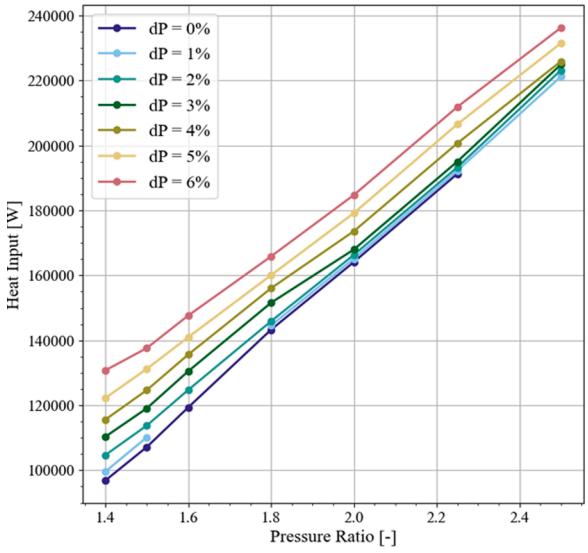

Fig. B2. Combustion heat required as a function of compressor pressure ratio for different combustion chamber pressure drop percentages – for the LTT setup with the GTX4088R (AR = 1.19) as the GT and the GBC14-200 as the PT

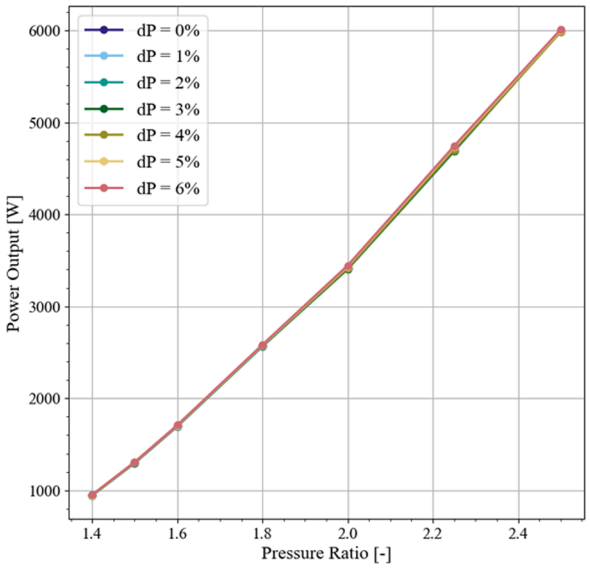

Fig. B3. Net power output as a function of compressor pressure ratio for different combustion chamber pressure drop percentages – for the LTT setup with the GTX4088R (AR = 1.19) as the GT and the GBC14-200 as the PT

Fig. B3 shows that the power output does not change much as the combustion chamber pressure drop changes. This is because the placement of the power turbine split-off point occurs before the combustion chamber and the power output is purely governed by the performance of the power turbine with only slight deviations occurring when the compressor performance changes due to the coupled nature of the compressor and gasifier turbine. Fig. B4 shows that the thermal efficiency decreases as the combustion chamber pressure drop increases. This is due to the increase in heat input with an increase in the pressure drop percentage. Both the power output and the thermal efficiency increase with an increase in the compressor pressure ratio.

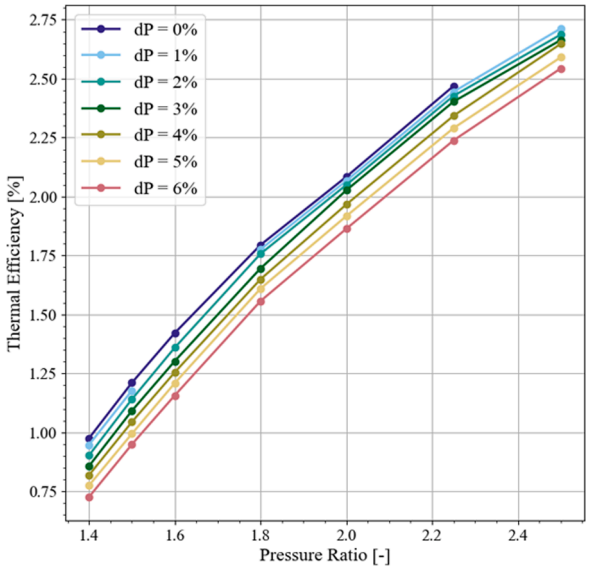

Fig. B4. Thermal efficiency as a function of compressor pressure ratio for different combustion chamber pressure drop percentages – for the LTT setup with the GTX4088R (AR = 1.19) as the GT and the GBC14-200 as the PT

Appendix C. Additional turbine inlet air cooling (TIAC) comparisons

Considering the model deviations, the TIAC cycles in the current study and in the study by Zaki et al. [19] cannot be directly compared as is. Therefore, for a comparison between the two cycles, a cycle with a similar setup to the Zaki et al. [19] cycle is simulated with the same conditions as the TIAC cycle discussed in the main section of the current study. This cycle, which is further referred to as the basic Zaki layout, follows a single-shaft gas turbine setup, with the parallel-flow TIAC cycle in Fig. 2 remaining mostly the same, and with the gasifier turbine inlet temperature being kept constant at 1200 K (this is the maximum limit of this temperature when *Garrett Motion* turbochargers are used). This cycle layout is further illustrated in Fig. C1. There is no indication of the coupling method used for the power turbine and compressor in the study by Zaki et al. [19]. Thus, it is assumed that these components are electrically coupled as this is the most feasible coupling method when considering the different shaft speeds that are applicable for the power turbine in comparison to the coupled gasifier turbine and compressor turbocharger pair. Note that no dehumidifier is included in this basic Zaki layout. Additionally, note that the basic Zaki layout makes use of two generators which requires additional capital expenditure to manufacture the cycle. Moreover, due to space restrictions, it is more difficult to mount a generator to the main shaft turbocharger.

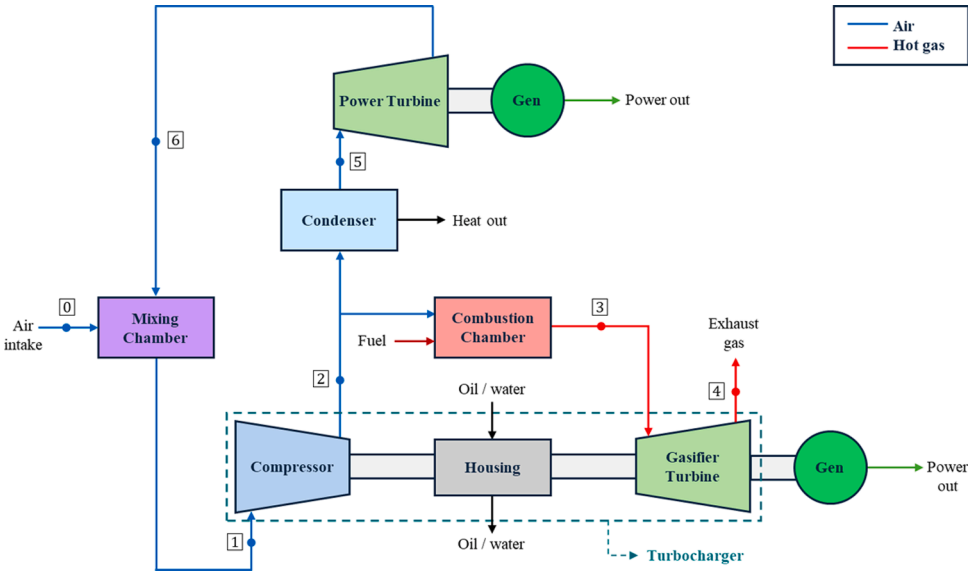

Fig. C1. Basic Zaki layout adapted from Zaki et al. [19].

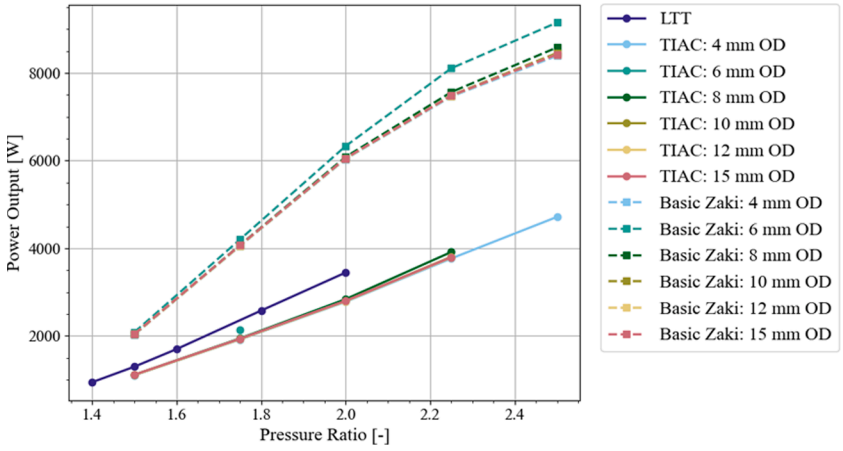

Fig. C2. Net power output as a function of compressor pressure ratio for the TIAC and basic Zaki setups with the G25-550 (AR = 0.92) as the GT and the GBC14-200 as the PT for different condenser tube outer diameters considering 30 condenser tubes

The thermal efficiency results comparison between the TIAC cycle, the LTT cycle, and the new basic Zaki layout are considered for the combination between the G25-550 (AR = 0.92) main shaft turbocharger and the GBC14-200 power turbine. For this, 30 condenser tubes are considered with a tube outer diameter of 8 mm, as in section 3.3. From Figs. C2 and C3, it is shown that for this analysis, the original basic Zaki layout offers much better power output, in comparison to both the LTT and the TIAC cycles in the current study, for the considered condenser geometries. Additionally, Figs. C4 and C5 show the same result with regard to thermal efficiency as the basic Zaki layout offers much higher thermal efficiency. This is as a result of the power output mostly being dictated by the gasifier turbine power generation rate in the basic Zaki layout, with some of the compressor power being supplemented by the power turbine. This does however mean that there is a greater expected reduction in power output under greater amounts of pressure loss in the components preceding the gasifier turbine in the basic Zaki layout due to the pressure ratios through both the power turbine and the gasifier turbine being influenced by pressure losses. This consideration is expected to have a minimal influence on the parallel-flow TIAC cycle due to only the pressure losses associated with the condenser influencing the pressure ratio through the power turbine. Note that the influence of the condenser geometry has the same effect on both the basic Zaki layout and the TIAC cycle, with a greater number of condenser tubes reducing the power output and thermal efficiency due to added cooling in both cycles. The effect of the condenser outer diameter on these cycle results is not as linear, as observed in sections 3.2 and 3.3.

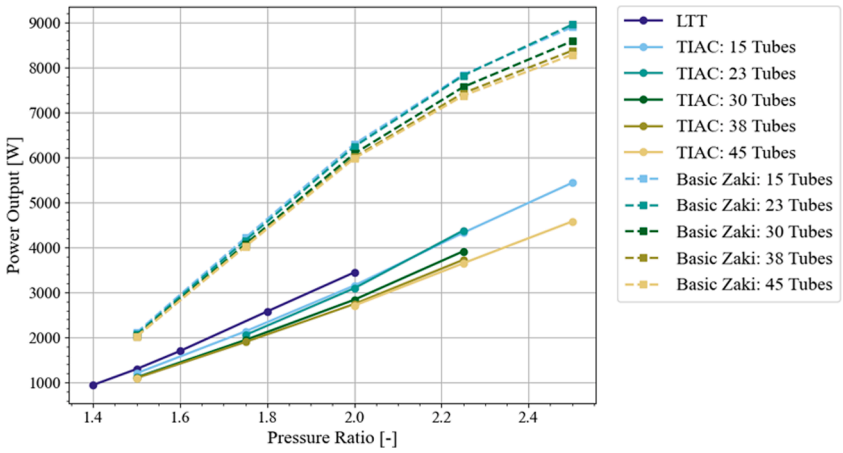

Fig. C3. Net power output as a function of compressor pressure ratio for the TIAC and basic Zaki setups with the G25-550 (AR = 0.92) as the GT and the GBC14-200 as the PT for different amounts of condenser tubes considering a condenser tube outer diameter of 8 mm

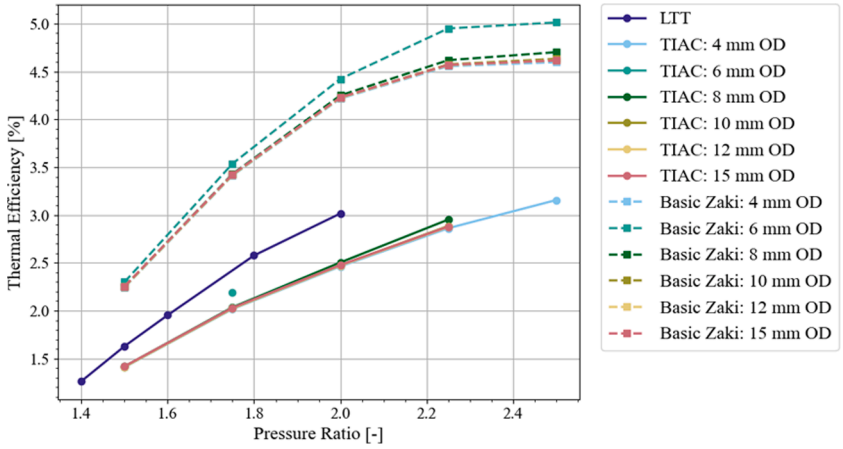

Fig. C4. Thermal efficiency as a function of compressor pressure ratio for the TIAC and basic Zaki setups with the G25-550 (AR = 0.92) as the GT and the GBC14-200 as the PT for different condenser tube outer diameters considering 30 condenser tubes

Overall, the basic Zaki layout has more potential than the TIAC cycle in the current study. This means that it is better to have a generator on the gasifier turbine as well than only having one on the power turbine in a simple cycle layout that does not include additional pressure loss components, such as recuperative heat exchangers, that are typically added to a cycle to improve the thermal efficiency of the cycle. This result may thus change when components are added to the cycle for the purpose of recuperation and/or solar hybridisation.

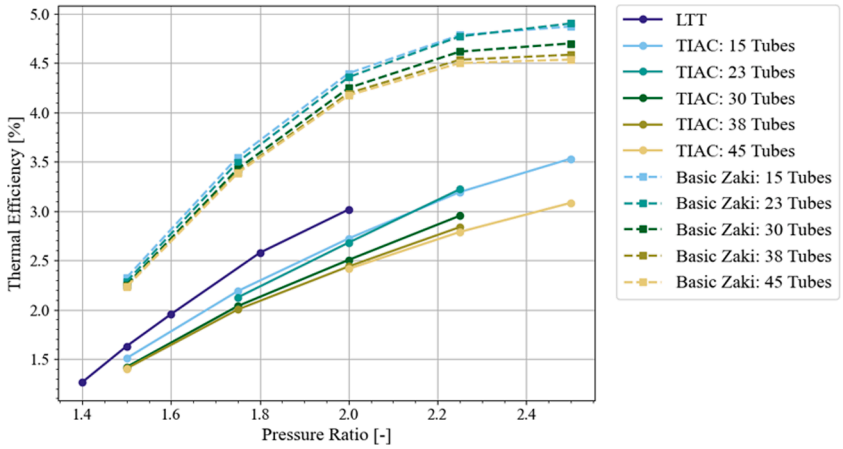

Fig. C5. Thermal efficiency as a function of compressor pressure ratio for the TIAC and basic Zaki setups with the G25-550 (AR = 0.92) as the GT and the GBC14-200 as the PT for different amounts of condenser tubes considering a condenser tube outer diameter of 8 mm

Data availability

Data will be made available on request.

References

[1] Gautam M, Tiwari A, Chauhan K, Fartyal G, Singh S, Chahar VK. The impact of ambient temperature on performance of simple Brayton cycle. Int J Mech Eng Technol (IJMET) 2017;8(4):75–81.

[2] A. Khademi, S. A. A. Mehrjardi, S. Tiari, K. Mazaheri and M. B. Shafii, "Thermal Efficiency Improvement of Brayton Cycle in the Presence of Phase Change Material," in *Proceedings of the 9th International Conference on Fluid Flow, Heat and Mass Transfer (FFHMT'22)*, Niagara Falls, Canada, 2022.

[3] Moradi A, Salehi G, Masoomi M, Manesh MHK. Performance analysis of gas turbine inlet air cooling plant with hybrid indirect evaporative cooling and absorption chiller system. Int J Thermodyn (IJoT) 2021;24(3):248–59.

[4] Hampel CA, Becker W, Olis D, Braun RJ. Evaluating the impact of off-design CHP performance on the optimal sizing and dispatch of hybrid renewable-CHP distributed energy resources. Energ Conver Manage 2024;306:1–21.

[5] El-Hadik AA. The impact of atmospheric conditions on gas turbine performance. J Eng Gas Turbines Power 1990;112(4):590–6.

[6] Baakeem SS, Orfi J, Al-Ansary H. Performance improvement of gas turbine power plants by utilizing turbine inlet air-cooling (TIAC) technologies in Riyadh, Saudi Arabia. Appl Therm Eng 2018;138:417–32.

[7] CITY OF TSHWANE, "2023–2024 REVIEW OF THE 2022-2026 INTEGRATED DEVELOPMENT PLAN," CITY OF TSHWANE, Pretoria, South Africa, 2024.

[8] Fellah GM. Effect of ambient temperature on the thermodynamic performance of a combined cycle. J Eng Res (Al-Fateh University) 2010;35(13):35–48.

[9] Jamal N. Options for the supply of electricity to rural homes in South Africa. J Energy Southern Africa 2015;26(3):58–65.

[10] Le Roux WG, Sciacovelli A. Recuperated solar-dish Brayton cycle using turbocharger and short-term thermal storage. Sol Energy 2019;194(2019):569–80.

[11] Kamal SNO, Salim DA, Fouzi MSM, Khai DTH, Yusof MKY. Feasibility study of turbine inlet air cooling using mechanical chillers in malaysia climate. Energy Procedia 2017;138:558–63.

[12] Zeitoun O. Two-stage evaporative inlet air gas turbine cooling. Energies 2021;14 (5):1–17.

[13] Maheshwari M, Singh O. Thermodynamic study of different configurations of gas-steam combined cycles employing intercooling and different means of cooling in topping cycle. Appl Therm Eng 2019;162.

[14] Chen L, Ni D, Zhang Z, Sun F. Exergetic performance optimization for new combined intercooled regenerative Brayton and inverse Brayton cycles. Appl Therm Eng 2016;102:447–53.

[15] Romier A. Small gas turbine technology. Appl Therm Eng 2004;24(11–12): 1709–23.

[16] Liu J, Zhang Y, Yin S, Zhang Y, Luo X, Liu Z. Economic and exergy transmission analysis of the gas-liquid type compressed CO2 energy storage system. Renew Energy 2024;230.

[17] Zhang W, Ding J, Yin S, Zhang F, Zhang Y, Liu Z. Thermo-economic optimization of an artificial cavern compressed air energy storgae with CO2 pressure stabilizing unit. Energy 2024;294.

[18] Arabi SM, Ghadamian H, Aminy M, Ozgoli HA, Ahmadi B, Khodsiani M. The energy analysis of GE-F5 gas turbines inlet air–cooling systems by the off-design method. Meas Control 2019;52(9–10):1489–98.

[19] Zaki GM, Jassim RK, Alhazmy MM. Brayton refrigeration cycle for gas turbine inlet air cooling. Int J Energy Res 2007;31(2007):1292–306.

[20] Van der Merwe AH, Le Roux WG, Humphries ED. Parallel turbochargers for small-scale power generation. Applied Thermal Engineering 2023:235. https://doi.org/10.1016/j.applthermaleng.2023.121410.

[21] W. G. Le Roux and J. P. Meyer, "Modeling the Small-Scale Dish-Mounted Solar Thermal Brayton Cycle," in *SOLARPACES 2015: International Conference on Concentrating Solar Power and Chemical Energy Systems*, Cape Town, South Africa, 2015. AIP Conf. Proc. 1734, 060002 (2016). DOI: https://doi.org/10.1063/1.4949144.

[22] De Beer JH, Le Roux WG, Sciacovelli A, Meyer JP. Effect of a novel cooling window on a recuperated solar-dish Brayton cycle. Renew. Energy 2023;208:465–80. https://doi.org/10.1016/j.renene.2023.02.085.

[23] Visser WPJ, Shakariyants SA, Oostveen M. Development of a 3 kW microturbine for CHP applications. J Eng Gas Turbines Power 2011;133(4):1–8.

[24] Bontempo R, Cardone M, Vorraro G. Steady and unsteady experimental analysis of a turbocharger for automotive applications. Energ Conver Manage 2015;99:72–80.

[25] T. Akba, D. K. Baker and M. Pınar Mengüç a, "Off-design performance of micro-scale solar Brayton cycle," *Energy Conversion and Management,* vol. 289, 2023.

[26] Kim J-S, Kim D-Y, Kim Y-T. Experiment on radial inflow turbines and performance prediction using deep neural network for the organic Rankine cycle. Appl Therm Eng 2019;149:633–43.

[27] Sadrehaghighi I. Components of an axial gas turbine engine. Research Gate 2023.

[28] Grönman A, Sallinen P, Honkatukia J, Backman J, Uusitalo A. Design and experiments of two-stage intercooled electrically assisted turbocharger. Energ Conver Manage 2016;111.

[29] Fatsis A. Design point analysis of two-shaft gas turbine engines topped by four-port wave rotors for power generation systems. Propul Power Res 2019;8(3):183–93.

[30] Garrett Motion, "Garrett Performance Turbo," 2023. [Online]. Available: https://www.garrettmotion.com/racing-and-performance/performance-turbos/?term_id=28. [Accessed 11 May 2023].

[31] Bell IH, Wronski J, Quoilin S, Lemort V. Pure and pseudo-pure fluid thermophysical property evaluation and the open-source thermophysical property library CoolProp. Ind Eng Chem Res 2014;53(6):2498–508.

[32] Le Roux WG, Bello-Ochende T, Meyer JP. Optimisation of an open rectangular cavity receiver and recuperator used in a small-scale solar thermal Brayton cycle with thermal losses, 10th. International Conference on Heat Transfer, Fluid Mechanics and Thermodynamics July, 2014 (HEFAT2014).

[33] Garrett Motion, "GARRETT G42-1200 73MM," 2024. [Online]. Available: https://www.garrettmotion.com/racing-and-performance/performance-catalog/turbo/g-series-g42-1200/. [Accessed 2 August 2024].

[34] C. Borgnakke and R. E. Sonntag, Fundamentals of Thermodynamics, 9th ed., Michigan: John Wiley & Sons, 2017.

[35] Automeris, "Extract data from charts," 2024. [Online]. Available: https://automeris.io/. [Accessed 2 August 2024].

[36] Ekwonu MC, Perry S, Oyedoh EA. Modelling and simulation of gas engines using aspen HYSYS. J Eng Sci Technol Rev 2013;6(3):1–4.

[37] B. Rankokwane, S. E. Makhurutha, T. Makhurutha and T. Motlasuping, "LIQUEFIED PETROLEUM GAS MARKET STUDY," Botswana Energy Regulatory Authority, Lobatse, 2021.

[38] H. Lefebvre and D. R. Ballal, Gas Turbine Combustion: Alternative Fuels and Emissions, 3rd ed., Boca Raton: Taylor and Francis Group, LLC, 2010.

[39] Kim WS. Design optimization of cross-counter flow compact heat exchanger for energy recovery ventilator. Int J Air-Conditioning Refrig 2022;30(16):1–15.

[40] Popoola OM, Burnier C. Solar water heater contribution to energy savings in higher education institutions: Impact analysis. J Energy Southern Africa 2014;25(1):51–8.

[41] H. E. Jacobs, B. E. Botha and E. J. M. Blokker, "Household Hot Water Temperature – An Analysis at End-Use Level," Kingston, 2010.

[42] H. Strauss, South African Tap and Flow Rate Gap Analysis, CLASP, 2022.

[43] Bitzer, "Water Cooled Shell and Tube Condensers," September 2018. [Online]. Available: https://www.bitzer.de/shared_media/documentation/dp-200-6-en.pdf. [Accessed 16 May 2023].

[44] Y. A. Çengel and A. J. Ghajar, Heat and Mass Transfer Fundamentals & Applications, 6th Edition in SI Units ed., Nevada: McGraw Hill Education, 2020.

[45] J. R. Thome, "Chapter 3: Single-Phase Shell-Side Flows and Heat Transfer," in *The Heat Transfer Engineering Data Book III*, Wolverine Tube, Inc., 2006, pp. 1-20.

[46] F. M. White, Fluid Mechanics, 8th ed., New York: McGraw-Hill Education, 2016.

[47] W. G. Le Roux; Feasibility study of a hybrid small-scale dish-mounted solar thermal Brayton cycle with cogeneration, 16th International Heat Transfer Conference (IHTC-16), Beijing, China, 10-15 August, 2018, DOI: 10.1615/IHTC16.nee.024185. pages 7929-7936.

[48] L. Guzzella and C. H. Onder, Introduction to Modeling and Control of Internal Combustion Engine Systems, 2nd ed., Heidelberg: Springer, 2010.